On the Role of Tropical Ocean Forcing of the Persistent North American West Coast Ridge of Winter 2013/14[a]

RICHARD SEAGER AND NAOMI HENDERSON

Lamont-Doherty Earth Observatory of Columbia University, Palisades, New York

(Manuscript received 17 February 2016, in final form 4 August 2016)

ABSTRACT

The causes of the high pressure ridge at the North American west coast during winter 2013/14, the driest winter of the recent California drought, are examined. The ridge was part of an atmosphere–ocean state that included anomalies, defined relative to a 1979–2014 mean, of circulation across the Northern Hemisphere, warm sea surface temperatures (SSTs) in the tropical western and northeastern Pacific and the south Indian Ocean, and cool SSTs in the central tropical Pacific. The SST anomalies differ sufficiently between datasets that, when used to force atmosphere models, the simulated circulation anomalies vary notably in realism. Recognizing uncertainty in the SST field, the authors use idealized tropical SST anomaly experiments to identify an optimal combination of SST anomalies that forces a circulation response that best matches observations. The optimal SST pattern resembles that observed but the associated circulation pattern is much weaker than observed, suggesting an important but limited role for ocean forcing. Analysis of the equilibrium and transient upper-troposphere vorticity balance indicates that the SST-forced component of the ridge arose as a summed effect of Rossby waves forced by SST anomalies across the tropical Indo-Pacific oceans and drives upper-troposphere convergence and subsidence at the west coast. The ridge, in observations and model, is associated with northward and southward diversion of storms. The results suggest that tropical Indo-Pacific ocean SSTs helped force the west coast ridge and drought of winter 2013/14.

1. Introduction

California experienced four consecutive drier than normal winters from 2011/12 to 2014/15 that pushed the state into a record multiyear drought that has had serious social, economic, environmental, and agricultural consequences (Howitt et al. 2014). Although intensified by long-term warming and coincident high temperatures (Williams et al. 2015), the root cause of the drought has been higher than normal pressure at the west coast of North America, which has gone along with fewer than normal winter storms bringing precipitation to California (Herring et al. 2014; Swain et al. 2014; Wang and Schubert 2014; Funk et al. 2014; Hartmann 2015; Seager et al. 2015). In an analysis of ensembles of SST-forced simulations conducted with seven atmosphere models by five institutions, Seager et al. (2015) provided evidence that in each of the 2011/12, 2012/13, and 2013/14 winters the west coast ridge and decreased precipitation had important contributions from forcing by global sea surface temperature (SST) anomalies, relative to a January 1979–April 2014 climatological mean. Winter 2011/12 was a La Niña event and hence the anomalous high pressure over the northeastern Pacific and dry conditions in southwestern North America were akin to the canonical response to La Niña events as in Seager et al. (2014a). Winters 2012/13 and 2013/14 were different and formally El Niño–Southern Oscillation (ENSO)-neutral. Despite this, the SST-forced models still tended to produce a west coast ridge and dry conditions at the coast, including California, but both of weaker amplitude than observed. Seager et al. (2015) argue that the ridge was partially forced by the tropical oceans via a mode of SST-forced variability, albeit one that explained less variance than ENSO or Pacific decadal variability. The SST-forced mode they identified

[a] Lamont-Doherty Earth Observatory Contribution Number 8057.

Corresponding author address: Richard Seager, Lamont-Doherty Earth Observatory of Columbia University, 61 Route 9W, Palisades, NY 10964.
E-mail: seager@ldeo.columbia.edu

DOI: 10.1175/JCLI-D-16-0145.1

had a west coast ridge associated with an increased SST gradient across the Pacific Ocean with warm anomalies in the western equatorial Pacific and weak cool anomalies in the central to eastern equatorial Pacific. This SST pattern seemed capable of exciting waves that propagated northeast to place a ridge at the North American west coast. However they also made clear that SST forcing could not fully explain the west coast ridge or the associated precipitation reduction and that internal atmosphere variability was likely to have been at least as important.

Since the winter of 2013/14 considerable work has been done to try to explain the causes of the unusual weather across the Northern Hemisphere. Hartmann (2015) came to a similar conclusion as Seager et al. (2015) based on observational and model analysis, and Davies (2015) also did via a potential vorticity analysis of transient weather systems. Lee et al. (2015) showed that many features of the observed circulation anomaly could be reproduced within an atmosphere model forced by the SST and sea ice anomalies that prevailed during the winter arguing for roles for tropical, extratropical, and subpolar forcing. On the other hand, Baxter and Nigam (2015) showed how the observed circulation anomalies could be understood in terms of known patterns of variability such as the western Pacific–North Pacific Ocean mode and argued for an origin in terms of internal midlatitude variability. They criticized Seager et al. (2015) for ''succumbing to the post 1980s–90s temptation'' of ascribing Pacific–North America variability to tropical sources and, together with Hartmann (2015), for failing to provide ''process-level observational support'' via, for example, analysis of outgoing longwave radiation or diabatic heating. Succumbing to temptation is not always a bad move and can lead to positive outcomes. Watson et al. (2016), in a modeling and observational study, showed that the warm SST anomalies in the tropical western Pacific Ocean did indeed correspond to positive precipitation anomalies (and therefore diabatic heating) and showed that this was one process, but by no means the only one, at play in generating the west coast ridge of winter 2013/14.

The work performed to date has pointed to answers in regard to generation of the west coast ridge that forced the California drought but leaves many questions unanswered. The current work extends beyond the prior work in terms of examining the physical processes involved in generating the SST-forced component of the ridge. Leading questions include the following: If we accept a limited role for ocean forcing, which we do, where is it in the global ocean that the forcing for the ridge originates? Is one region with a simple wave response (e.g., the tropical western Pacific) or multiple regions with superimposed or interacting waves responsible? What are the anomalies in the location and intensity of precipitation-bearing North Pacific storm track associated with the ridge? What are the physical mechanisms of wave–mean flow–transient eddy interaction that connect the SST anomalies to the west coast ridge and suppression of precipitation? Further, once the culprit ocean state has been identified, what ocean–atmosphere processes were responsible for creating that state? Here we will address the first three questions and leave the fourth oceanographic question aside while noting that for the general problem of drought far less attention is paid to the causes of the responsible SST anomalies than to the atmospheric response to them.

Here we report on a series of modeling experiments designed to understand the non-ENSO ocean forcing contribution to the west coast ridge focusing in on winter 2013/14 as the more extreme of the two years that had this feature. Given the results in Seager et al. (2015) we can only hope to explain the component of the west coast ridge in winter 2013/14 that was SST forced and not its entirety. It is found here that the usual methodology to identify ocean forcing of imposing actual SST anomalies by ocean basin and region in order to locate the prime forcing region for the response feature of interest does not work well for the case of winter 2013/14. Reasons for this are discussed and in part relate to uncertainties in the SST field itself that may have affected the model-based analyses by the prior workers mentioned above. Recognizing this, we turn to a series of idealized SST forcing experiments and use an optimization procedure to identify the combination of tropical SST and associated diabatic heating forcing that leads to the best match for the observed circulation anomaly. The implied SST and precipitation anomalies are compared to those observed and linearity is assessed by rerunning the model forced by the optimal SST forcing pattern. The modeling experiments implicate a collection of SST anomalies in the Indian and tropical Pacific Oceans as combining to help force the west coast ridge and drought of winter 2013/14. We then study the observed and modeled upper-troposphere vorticity balance to understand the physical mechanisms that underlay the persistent west coast ridge. To complete the study we then analyze the transient day-by-day and week-by-week adjustment of the atmospheric circulation and vorticity balance in response to the switching on of the optimal SST forcing field, allowing cause and effect to be successfully diagnosed. By design, the optimization methodology determines an upper bound on the SST-forced contribution to the ridge. Even so, this is weaker than

observed. Analysis of the ensemble members supports the idea that internal atmosphere variability combined with the SST forcing to determine the amplitude and pattern of this extreme event.

2. Observational data and model simulations

a. Observations

For anomalies in the atmospheric circulation during winter 2013/14 we use the National Centers for Environmental Prediction (NCEP)–National Center for Atmospheric Research (NCAR) reanalysis [Kistler et al. 2001; accessed from the International Research Institute for Climate and Society (IRI) data library at http://iridl.ldeo.columbia.edu/expert/SOURCES/NOAA/NCEP-NCAR/CDAS-1/MONTHLY/] and the European Centre for Medium-Range Weather Forecasts (ECMWF) interim reanalysis (ERA-Interim; Berrisford et al. 2011a,b; Dee et al. 2011; accessed from http://www.ecmwf.int/en/research/climate-reanalysis/era-interim). To analyze global precipitation we use the satellite-gauge data from both the Global Precipitation Climatology Project (GPCP; Adler et al. 2003; accessed from the IRI data library at http://iridl.ldeo.columbia.edu/SOURCES/NASA/GPCP/V2p2/satellite-gauge/) and the Climate Prediction Center (CPC) Merged Analysis of Precipitation (CMAP; Huffman et al. 1997; Adler et al. 2003; accessed from the IRI data library at http://iridl.ldeo.columbia.edu/SOURCES/NOAA/NCEP/CPC/Merged_Analysis/monthly/latest/ver2/). The most recent issues of each precipitation data were used. For SST we analyzed the Hadley Centre Sea Ice and Sea Surface Temperature (HadISST) data product (Rayner et al. (2003); accessed from http://www.metoffice.gov.uk/hadobs/hadisst/data/download.html), the National Oceanic and Atmospheric Administration (NOAA) Extended Reconstructed SST version 4 data (ERSST.v4; Huang et al. 2015; accessed from http://iridl.ldeo.columbia.edu/SOURCES/NOAA/NCDC/ERSST/version4/) and the ECMWF Ocean Reanalysis System 4 (ORAS4) of Balmaseda et al. (2013; accessed from https://reanalyses.org/ocean/overview-current-reanalyses). Surface latent and sensible heat flux data are from Yu et al. (2008; accessed from http://oaflux.whoi.edu/data.html), and make use of surface and satellite information and are referred to herein as the OA fluxes. All monthly anomalies are relative to a January 1979–April 2014 climatology.

b. Models

The atmosphere model we use is the NCAR Community Climate Model, version 3 (CCM3; Kiehl et al. 1998), run at spectral T42 resolution with 19 vertical levels. CCM3 is a vintage model but has been the workhorse model at Lamont for over a decade and found to compare favorably with the more recent Community Atmosphere Model (CAM) versions for simulation of tropical forcing of North American hydroclimate. Since CCM3 also uses about one-twentieth the computing time of the CAM versions, allowing for large ensembles and numerous experiments, we will use the vintage CCM3 once more here. It was used for the 16-member SST-forced ensembles run from 1856 to the present, the analysis of which has led to considerable advances in understanding North and South American drought history (Seager et al. 2005, 2009, 2010a) and has also been applied to understanding the evolution of transient eddy–mean flow interaction over the Pacific–North America region during ENSO events (Seager et al. 2010b). The sensitivity of the atmospheric responses to different observed estimates of the DJF 2013/14 SST anomaly was also assessed with the NCAR Community Atmosphere Model, version 5.3 (CAM5.3), also run at spectral T42 resolution with 30 levels.

We conduct two types of modeling experiments:

1) The 100-member ensembles forced by historical observed SST anomalies during December 2013–February 2014 were generated using different SST datasets as forcing. The ensemble mean is analyzed as an anomaly relative to the January 1979–April 2014 climatology of a 16-member ensemble forced with Hadley Centre SSTs. The 100 ensemble members are initialized on 1 December 2013 with different initial conditions taken from 1 December atmospheric and land surface states of long model simulations with repeating climatological Hadley Centre SSTs.
2) The 100-member ensembles simulating the 100 days beginning 1 December in which fixed idealized SST anomalies are added to the Hadley Centre SST climatology. An additional 100-member ensemble was generated using the same atmosphere and land initial conditions but climatological SSTs. The ensemble means of the daily differences between the 100 perturbed and control pairs were then analyzed. The perturbed simulations are forced by ''box-SST anomalies'' centered on the equator at different longitudes from the Indian Ocean to the eastern tropical Pacific. Each anomaly has a maximum of 1°C and is in a box centered on the equator stretching from 10°S to 10°N and spanning 30° in longitude. One pass of a 1–2–1 smoother in space was applied to the anomalies to remove the sharp SST anomaly gradients at the box edges. Experiments were run for both warm and cold SST anomalies with

results shown for the warm minus cold experiments divided by two.

3. Atmosphere–ocean conditions during winter 2013/14

We focus on the winter of 2013/14, which was the driest, as measured by all of California, November through April precipitation reduction, so far in the current California drought (Seager et al. 2015). We also focus on the December through February (DJF) season at the heart of winter.

a. *Observed and reanalysis SST, surface flux, precipitation, and circulation anomalies*

Figure 1 shows the observed 200-mb height and precipitation anomalies (1 mb = 1 hPa) from the NCEP–NCAR reanalysis and ERA-Interim, the GPCP and CMAP precipitation anomalies, the ERSST.v4 SST anomaly, and the latent plus sensible OA flux anomaly for DJF 2013/14. The height anomaly, which is very similar for both reanalyses, includes a north-northwest–south-southeast-oriented ridge immediately west of the North American coast and extending from Alaska to Mexico. The ridge is part of a more general area of high geopotential heights that extends west over the North Pacific, Bering Sea, and eastern Siberia. There was also a deep trough centered over Hudson Bay, responsible for the very cold winter in northeastern North America (Hartmann 2015; Baxter and Nigam 2015), low heights over the midlatitude North Atlantic, and high heights over the subtropical North Atlantic (although not with the canonical positive North Atlantic Oscillation pattern).

The precipitation anomaly associated with this height pattern shows the dry conditions along the U.S. west coast and expanding into British Columbia, northwestern Mexico, and the central United States. The west coast and central North America dry anomalies are under northerly upper-level flow. Over the North Pacific, wet anomalies occur on the western, southerly, flowing flank of the ridge and another dry anomaly under northerly flow over the northwestern Pacific. In the tropics there was a dry anomaly over the central–eastern Pacific, a wet anomaly northwest of Papua New Guinea, generally neutral to dry conditions over the Maritime Continent, and wet conditions over the west-central Indian Ocean. These features are common across the four precipitation estimates but there are some notable differences in the amplitude and pattern between the datasets. For example, the NCEP–NCAR reanalysis has a more coherent western Pacific–Maritime Continent wet anomaly but not the wet Indian Ocean anomaly seen in the other three estimates.

In the reanalysis-based moisture budget analysis of Seager et al. (2014b), precipitation at the west coast of North America arises from westerly winds, orographic uplift at the coast, and the propagation onshore from the west of storm systems within the Pacific storm track. Further, Seager et al. (2014b) also show that interannual variability of the moisture convergence by transient eddies is very important, especially for producing precipitation in southern California and northern Mexico in winter. The west coast ridge of winter 2013/14 and the associated lack of storm systems impinging on the west coast of the United States was responsible for the dry conditions. A measure of the storm-track activity is the high-pass filtered upper-tropospheric meridional velocity variance. Using daily data from the NCEP–NCAR reanalysis we computed this using a fourth-order Butterworth filter with a 10-day cutoff and the middle-right panel of Fig. 1 shows the anomaly for DJF 2013/14. There was a rather striking banded structure across the eastern North Pacific and North America with reduced eddy activity centered around the latitude of California and increased activity to the north. This implies fewer and/or weaker storms entering the southern portions of the west coast and, along with the mean high pressure ridge, is consistent with reduced precipitation (and the California drought).

The SST anomaly during DJF 2013/14 (contours in the middle-left panel of Fig. 1, colors in Fig. 2) shows cool anomalies in the central to eastern tropical Pacific, warm anomalies in the western tropical Pacific, a broad region of warm anomalies in the Indian Ocean south of the equator,[1] and a remarkably warm anomaly in the northeastern Pacific south of Alaska and west of British Columbia and Washington state. The colors in the middle-left panel of Fig. 1 are the surface latent plus sensible heat flux, defined here as positive into the ocean. Notably the warm North Pacific SST anomalies are associated with anomalous flux of heat into the ocean (i.e., atmospheric forcing of the anomalies). Further, Bond et al. (2015) performed an ocean mixed layer heat budget analysis of the northeastern Pacific warm anomaly and found that the prime driver of it was a reduction in entrainment of cool water into the mixed layer as a consequence of extreme low wind speeds. Hence, via both surface fluxes and mixed layer processes, the northeastern Pacific warm anomaly appears as a result of the west coast ridge and not a driver. In contrast, the warm SST anomaly in the tropical western Pacific was associated with an anomalous flux of latent

[1] The Indian Ocean warm SST anomalies strengthen to the south of the domain shown but were not associated with increased precipitation that would force an atmospheric response.

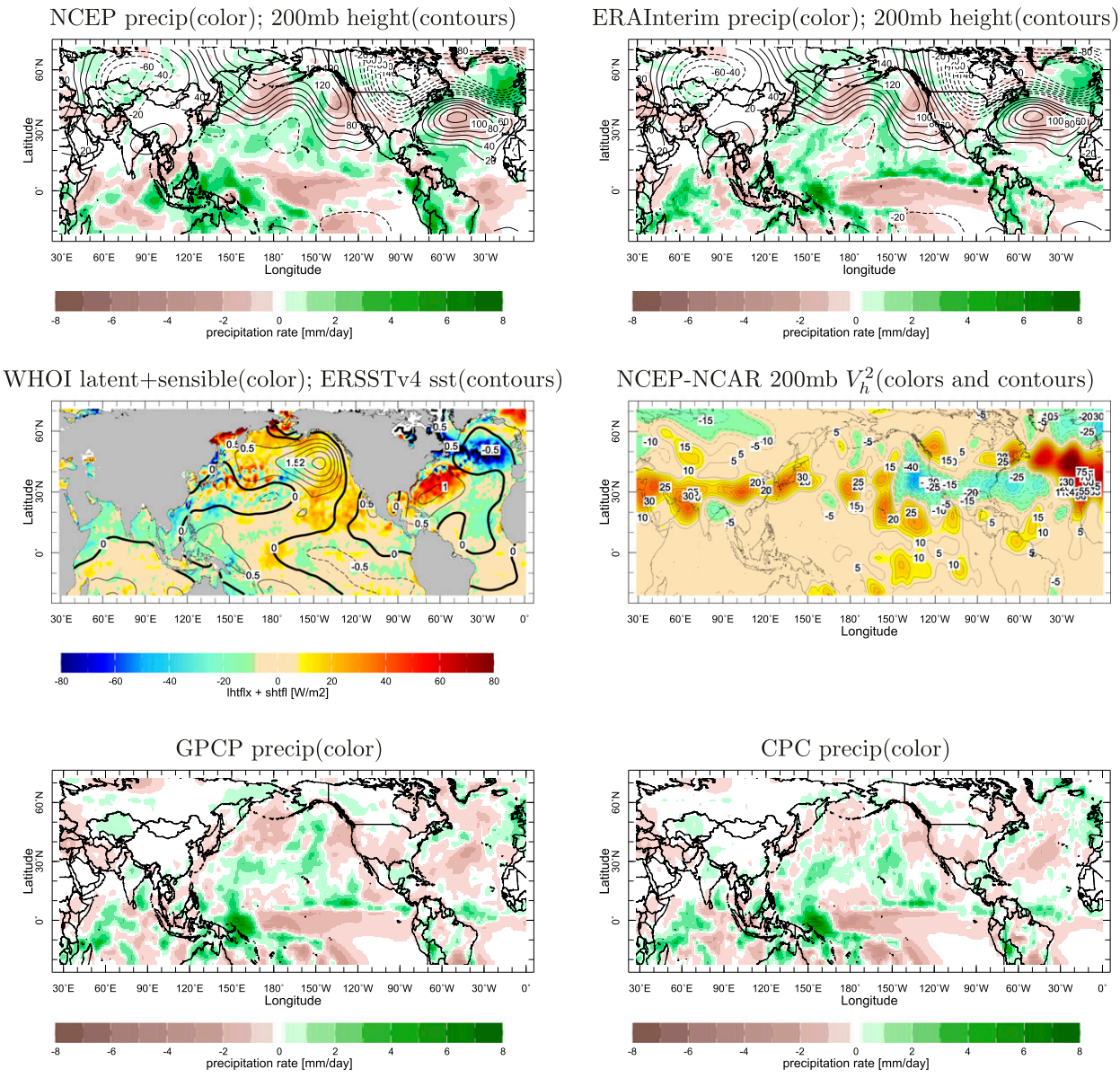

FIG. 1. The 200-mb height (m) and precipitation anomalies (mm month^{-1}) from the (top left) NCEP–NCAR reanalysis (top right) and ERA-Interim, (middle left) SST from ERSST.v4 (K) and OA flux data of surface latent plus sensible surface heat flux (positive into the ocean; W m^{-2}) anomalies, (middle right) NCEP–NCAR reanalysis high-pass-filtered 200-mb meridional velocity variance anomaly (m^2 s^{-2}), and (bottom left) GPCP and (bottom right) CMAP satellite–gauge precipitation anomalies (mm month^{-1}) all for DJF 2013/14.

plus sensible heat from the ocean to the atmosphere. There is also a region on the equator at the date line of anomalous ocean heat uptake. This corresponds to a region of negative precipitation anomaly in the GPCP data but is at the border between positive and negative SST anomalies in the ERSST.v4 analysis.

These associations are suggestive of ocean driving of the atmosphere in the tropical western Pacific and the opposite over the North Pacific, an entirely familiar state of affairs in interannual climate variability that has been well known dating back to Alexander (1992a,b), Cayan (1992), and Lau and Nath (1994, 1996). However, it

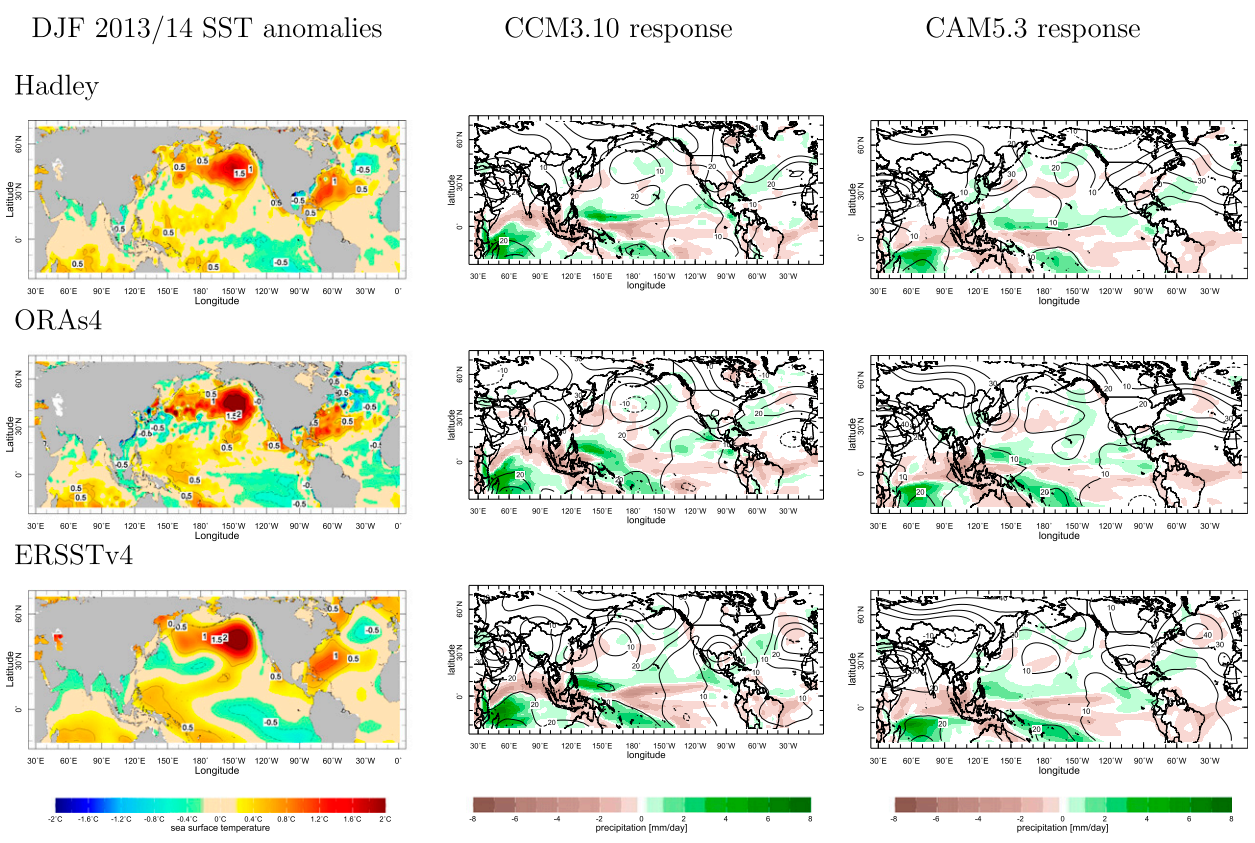

FIG. 2. (left) The observed DJF 2013/14 SST anomalies (K) from the (top) HadISST, (middle) ORAS4, and (bottom) ERSST.v4 datasets, and the 100-member ensemble mean 200-mb height (contours; m) and precipitation (colors; mm day^{-1}) response of (center) CCM3 and (right) CAM5.3 to the SST anomalies when imposed on the same SST climatology. For the height fields, the contour interval is 10 m with the zero contour suppressed.

should be noted that what the SST anomaly was during DJF 2013/14 is not clear. Figure 2 (left panels) shows maps for the anomaly, all relative to the same 1979–2014 climatology, for the HadISST, ORAS4, and ERSST.v4 datasets. All three disagree on the amplitudes of the warm SST anomalies in the North Pacific (by about 0.5 K) and in the tropical western Pacific and the cold anomaly in the central equatorial Pacific Ocean (typically by less than 0.5 K). Some of this disagreement is to be expected since the ERSST.v4 dataset only uses in situ measurements while HadISST and ORAS4 also use satellite data (but with different sources) and the analysis methods used to obtain gridded datasets differ.

b. *Atmosphere model response to observed estimates of SST anomalies*

The differences in the SST anomalies matter for the atmospheric response. Figure 2 shows the modeled ensemble mean 200-mb height and precipitation response to the DJF 2013/14 global SST anomalies when the HadISST, ORAS4, and ERSST.v4 anomalies are added to the Hadley Centre climatological SST for CCM3 (center panels) and CAM5.3 (right panels). Five of the six combinations of SST forcing and model have high height anomalies near or at the west coast, with CAM5.3 and Hadley Centre SST forcing the exception. The elongated northwest to southeast orientation of the ridge is most realistic with the ORAS4 SST forcing. The Hudson Bay trough is only produced with ORAS4 SST forcing within CCM3. The height anomalies are, as expected, considerably smaller than observed, consistent with SST forcing only being partially responsible for the ridge. The associated precipitation anomalies also largely agree with the observations with dry across the central–eastern tropical Pacific, wet over the western tropical Pacific. However, with Hadley Centre SST forcing in particular, the western tropical Pacific wet anomaly is split in two by a westward extension of the equatorial Pacific dry zone. The models also have unrealistic dry anomalies over the Maritime Continent. The model simulations all agree on wet conditions over the southern Indian Ocean and dry conditions to the north, which is clearly a simple response to the warm (cold) southern (northern) Indian Ocean SST anomalies

but which is only hinted at in the GPCP observed precipitation anomaly. The responses in heights and precipitation of the two atmosphere models are quite similar and both models show the sensitivity to choice of SST forcing dataset.

Despite the noted aspects of model–observation agreement all three forced responses differ. This is despite the experiments being done with the same model and with the anomalies being imposed on the same SST climatology and the ensemble containing 100 members, which effectively isolates the forced response. The differences between the responses to the three SST anomaly estimates appearing in each atmosphere model indicates that the differences in SST anomalies matter and, of course, we cannot tell easily which SST dataset is more accurate. It is sobering to realize that, in this important case, modern observations and analysis methods cannot constrain SST anomalies to the accuracy required to successfully model the atmospheric response.

An additional problem with SST-forced experiments for winter 2013/14 concerns the North Pacific warm SST anomaly. In experiments we have performed with SST forcing restricted to the tropics only and the North Pacific only, it is clear that the response to global SSTs seen in Fig. 2 involves both. However, when the North Pacific SST anomaly is imposed alone the atmosphere model responds by increased ocean to atmosphere surface heat flux, northerly winds above [which can balance the heating with advective cooling as in Hoskins and Karoly (1981)], and a high to the west. This response is essentially the opposite of the flow–flux relationship seen in observations during DJF 2013/14 [Fig. 1; see also Bond et al. (2015)] and is consistent with being a spurious model response to an imposed SST anomaly that was in fact generated by the atmospheric flow pattern. All of the simulated responses in Fig. 2 will be corrupted by some element of this spurious response.

c. *On the difference in amplitude of observed and modeled circulation anomalies*

In addition to being different from one another all the model circulation responses are much weaker than the observations. We found that the observed west coast ridge height anomaly is about 1.5 times the standard deviation of the DJF seasonal mean height anomalies. In contrast the modeled ensemble mean 60-day average height anomaly at the west coast is only about half of the standard deviation of 60-day mean height anomalies across the 100-member ensemble. These relative values are consistent with the suggestion of Seager et al. (2015) that only about one-third of the circulation anomaly could be explained in terms of SST forcing, leaving the rest to be explained by internal atmospheric variability. The relatively small SST-forced signal to atmospheric noise ratio means that a large ensemble (e.g., 100 members) is required to capture the response in the ensemble mean.

4. Constructive modeling of the west coast ridge of winter 2013/14

The above results and arguments make clear that we cannot expect to explain the origin of the circulation anomalies of DJF 2013/14 by simply imposing an ''observed'' SST anomaly as the lower boundary condition for an atmosphere model. Instead we will adopt a more roundabout route that seeks to identify a combination of idealized SST and associated diabatic heating anomalies that can reproduce the circulation anomaly.

a. *Box-SST anomaly experiments*

Turning to the results of the box-SST anomaly modeling experiments, we begin by noting that the circulation of DJF 2013/14 is unlike any familiar wave trains produced by these localized SST anomalies. Figure 3 shows the 200-mb geopotential height anomaly responses (right panels) to the imposed box-SST anomalies (left panels). A warm SST anomaly in the central equatorial Pacific Ocean (Fig. 3, fourth row) forces a single wave train that is quite characteristic of El Niño events with a low height anomaly over the North Pacific and a high anomaly centered over western Canada. The same size SST anomaly to the east (Fig. 3, bottom panel) is less effective at forcing a response in the height field. As the warm anomaly is moved west the response moves west too but also weakens and then changes character when the warm SST box is placed in the Indian Ocean. In that case (Fig. 3, top panel) a rather zonally symmetric response results with low height anomalies over northern Canada and high height anomalies over the North Pacific and North Atlantic, somewhat reminiscent of the warm Indian Ocean–positive North Atlantic Oscillation connection identified by Hoerling et al. (2001). The observed DJF 2013/14 height anomaly is not very akin to any of these patterns, or their opposite, but instead is more akin to some combination of these anomalies, indicating that SST anomalies across the Indo-Pacific oceans may have collectively contributed to the circulation anomaly.

b. *Optimal combinations of box-SST anomaly responses that match DJF 2013/14*

Given that the circulation of DJF 2013/14 cannot be easily explained as a response to a single localized SST anomaly, can it be explained as a combination of wave

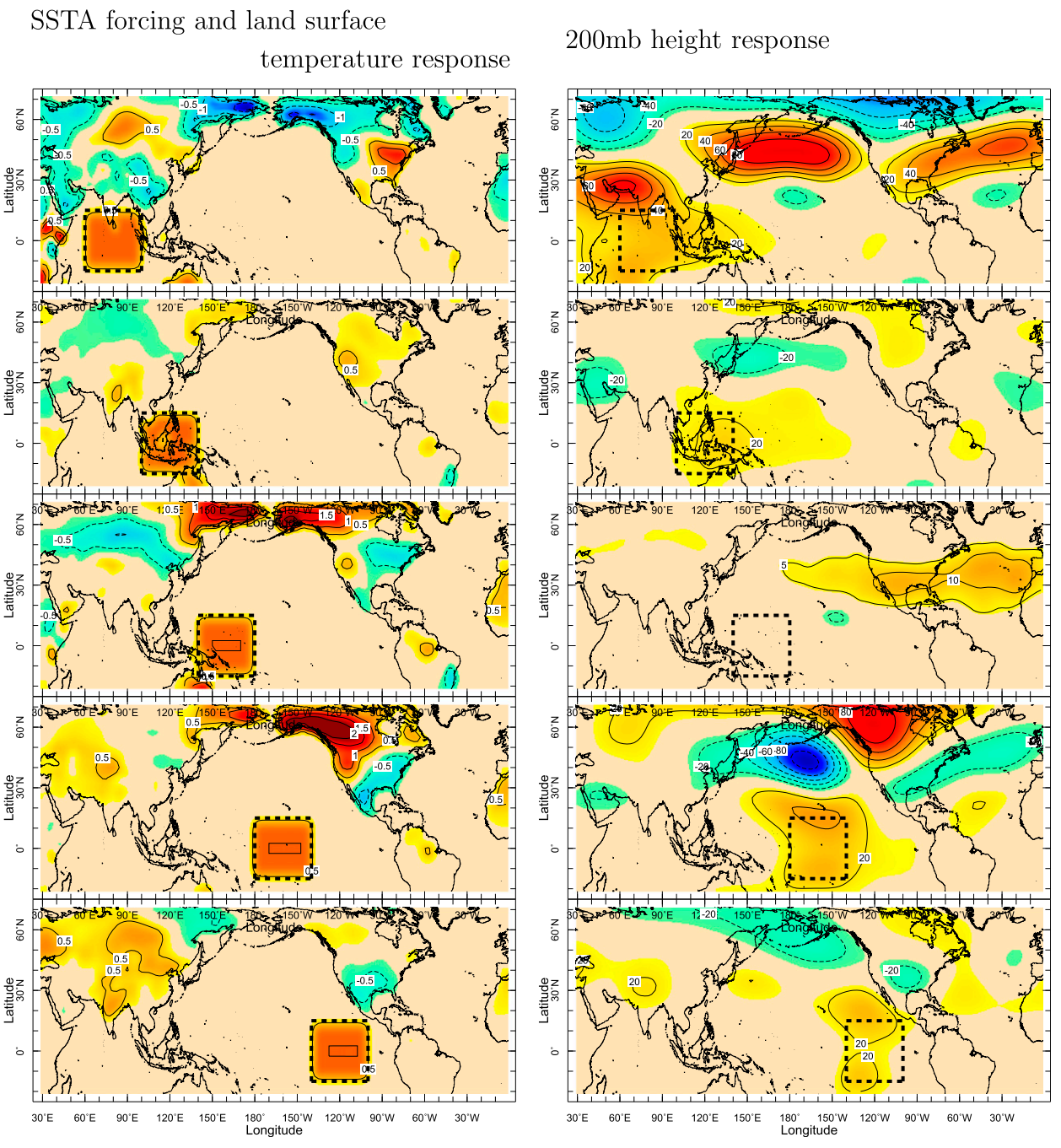

FIG. 3. (left) The imposed "box-SST anomalies" (K) and (right) the 100-member ensemble mean 200-mb height response (m). The SST anomalies were imposed upon a DJF SST climatology and the average is over days 40–100 of 100-day simulations initiated on 1 December. In (left) the modeled land surface temperature response (K) is also shown.

responses to a variety of SST anomalies and, if so, can this be understood in terms of linear superposition of the different waves? To assess this we seek the optimal linear combination of box-SST-anomaly response patterns that best matches the observed DJF 2013/14 200-mb height anomaly for all longitudes and from 25° to 75°N. This map Z'_{NCEP} is our target pattern and is a subset of the field shown in Fig. 1.

We denote the 200-mb heights from the box-SST anomaly experiments as Z_j. We use a constrained linear least squares optimization to find the best approximation of the Z'_{NCEP} using linear combinations of the Z'_j with the

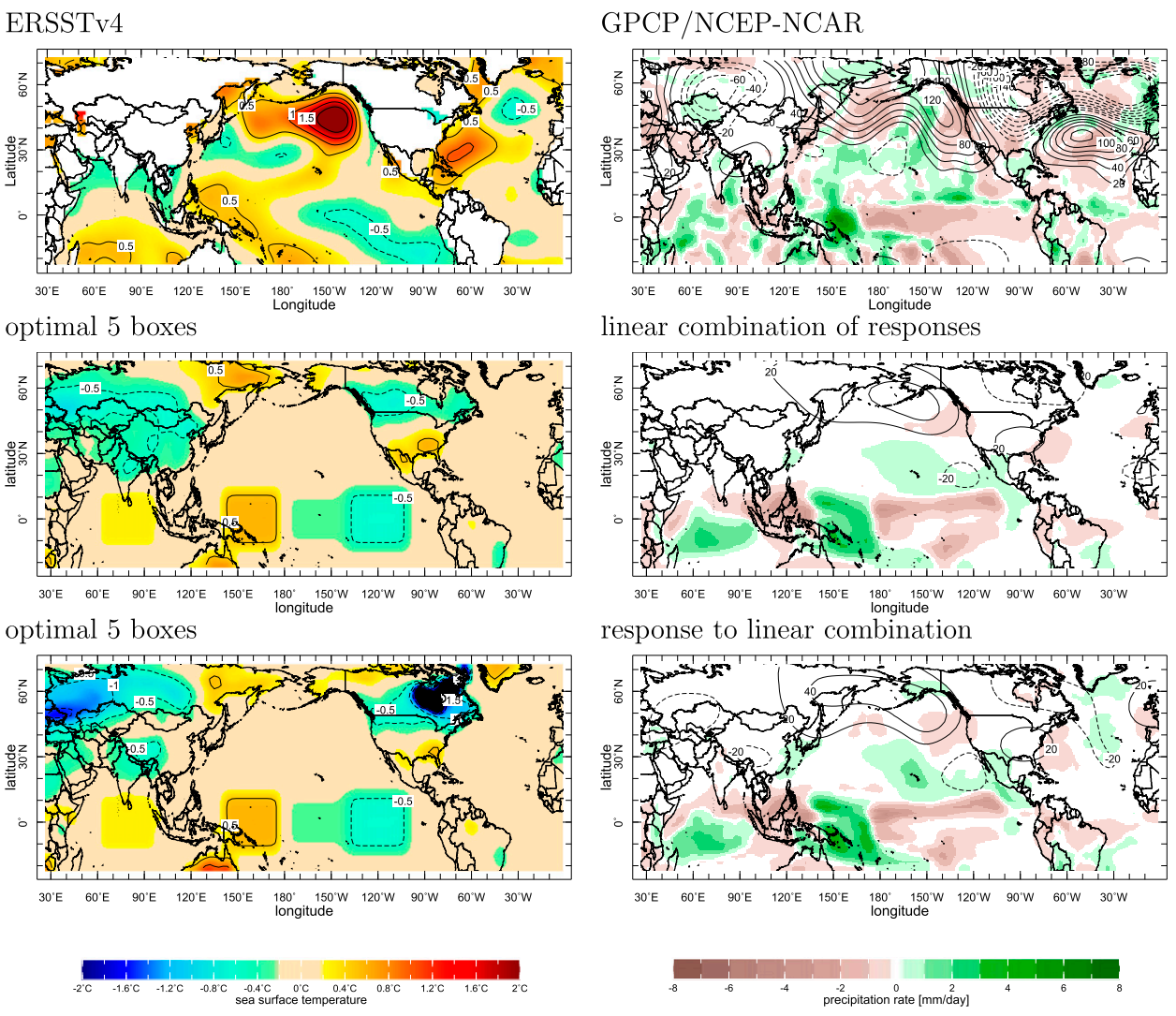

FIG. 4. (top left) The ERSST.v4 observed SST anomaly (K) and (top right) the GPCP observed precipitation (colors; mm day^{-1}) and NCEP–NCAR reanalysis 200-mb height (contours; m) anomalies for DJF 2013/14. (middle) As in (top), but constructed with the optimal sum of the box-SST anomaly forcing experiments, including modeled land surface temperature response (K); (bottom) as in (middle), but for the single ensemble forced by the corresponding constructed SST anomaly.

realistic constraint that the SST anomalies are less than 0.6 K. This can be expressed as the problem of finding N constants c_j, which achieve the distance minimization:

$$\min_{c}\left(\left\|\sum_{j=1}^{N} c_j Z'_j(\mathbf{x}) - Z'_{\mathrm{NCEP}}(\mathbf{x})\right\|\right), \tag{1}$$

subject to the constraint

$$|c_j| \le 0.6, \tag{2}$$

where the global area-weighted energy norm over all grid points $\mathbf{x} = (\lambda, \phi)$, where λ is longitude and ϕ is latitude, is

$$\|f(\mathbf{x})\|^2 \equiv \frac{\sum_{\mathbf{x}} f^2(\mathbf{x})\cos\phi}{\sum_{\mathbf{x}} \cos\phi}.$$

Finding the c_j for $j = 1, ..., 5$ from the above procedure produces the 200-mb height anomaly pattern shown in Fig. 4. The optimization is able to create a west coast–North Pacific ridge and also a weak Hudson Bay trough pattern that, although far from a perfect match, has clear similarities to that observed despite being much weaker. The differences in structure (including the ridge not extending far enough south) and amplitude support the idea that the observed pattern combines an SST-forced response with constructive internal atmosphere variability.

Agreement between observed and modeled height anomalies is poor over Asia and the North Atlantic, perhaps indicating an even greater role there for internal atmospheric variability in explaining the observed pattern. Figure 4 also shows the corresponding SST and precipitation anomalies, derived from the same linear combination of box-SST anomaly experiments. The optimal circulation anomaly arose as a response to a collection of SST anomalies and associated precipitation anomalies. The best match to observations requires a modestly warm eastern Indian Ocean, with temperatures near normal over the Maritime Continent region, warm in the western tropical Pacific Ocean, and cool across the central and eastern tropical Pacific Ocean. The precipitation anomalies the model produces closely match the SST anomalies in a warm and wet or cool and dry sense as expected, and also have some similarity to the observed precipitation anomalies in Fig. 1 although the Indian Ocean wet anomalies appear too large. It is noteworthy that, out of all the possible combinations of sign, amplitude, and location of SST anomalies that the optimization could have chosen to find a response field that best matches the observed height field, it chose one that has a clear resemblance to reality.

c. *Checking for linearity of the response to collections of SST anomalies*

Identifying a linear combination of box-SST anomaly responses that best matches the observed circulation does not mean that, if forced with the associated linear combination of SST anomalies, the atmosphere model would reproduce the same circulation. This is because the model is nonlinear and allows for the possibility that the waves forced from the various ocean regions will interact with each other to produce a response that departs from the linear assumption. To check this we forced the atmosphere model with the optimal linear combination SST pattern and the results are shown in the bottom panel of Fig. 4. The model 200-mb height response to the optimized SST anomalies is quite similar in the important details to the optimal sum of the individual box experiments, confirming the basic linearity of the response. That is, the total response can be understood as the linear combination of waves forced by the components of the total SST anomaly field with little important interaction between the forced waves.

5. Tropical Indo-Pacific SST anomaly forcing of circulation and storm-track anomalies in the eastern North Pacific and North America sector

Tropical SST anomalies can exert a strong influence on the strength and latitude of the Pacific storm track over the eastern North Pacific and west coast of North America. Returning to the box-SST anomaly experiments, Fig. 5 shows the ensemble mean change in the 200-mb high-pass-filtered meridional velocity variance averaged over days 40–100 of each experiment. Depending on where the SST anomaly is located it can have quite different effects on the Pacific storm track. For a warm SST anomaly in the central equatorial Pacific a rather classic El Niño–like southward displacement and strengthening of the storm track from the central North Pacific to North America occurs as analyzed in detail in Seager et al. (2010b) and Harnik et al. (2010). The argument in those papers is that the storm-track displacement occurs as the transient eddies are refracted more equatorward as a consequence of strengthened subtropical westerly winds that occur poleward of the diabatic deep convective heating anomaly generated by the warm SST anomaly. A warm SST anomaly in the far-western tropical Pacific generates a similar but weaker southward storm-track displacement. In contrast, a warm SST anomaly in the Maritime Continent region induces only a weak response whereas one over the Indian Ocean causes a strong poleward displacement with increased eddy activity over British Columbia and Alaska and decreased activity over California and Mexico.

Returning to Fig. 1 (middle-right panel), it is seen that winter 2013/14 had a reduction of eddy activity centered over the eastern North Pacific and North America at the latitude of California with increased activity over southwestern Canada and over the subtropical eastern North Pacific. From Fig. 5, this would appear to be a pattern that could be induced by a combination of tropical SST anomalies, including a warm anomaly over the western tropical Pacific, which can cause a reduction of eddy activity at the location of California and an increase over the subtropical North Pacific Ocean extending to the south of California.

Figure 6 shows the evolution of the mean and transient circulation response in the model forced by the switching on of the optimized SST anomaly pattern. Here the ensemble mean anomaly will, over the 10–15-day time period of initial value predictability when the ensemble members closely resemble each other, represent the daily evolution of the forced response to the imposed SST anomaly and hence we show daily values. After that, the ensemble members will diverge and we show time averaged quantities to identify more closely the SST-forced response. The initial response involves positive height anomalies straddling the equator over the western Pacific Ocean and negative height anomalies straddling the central Pacific Ocean: classic Gill (1980) responses to convection and vertical motion anomalies above warm and cool SST anomalies. By day 8

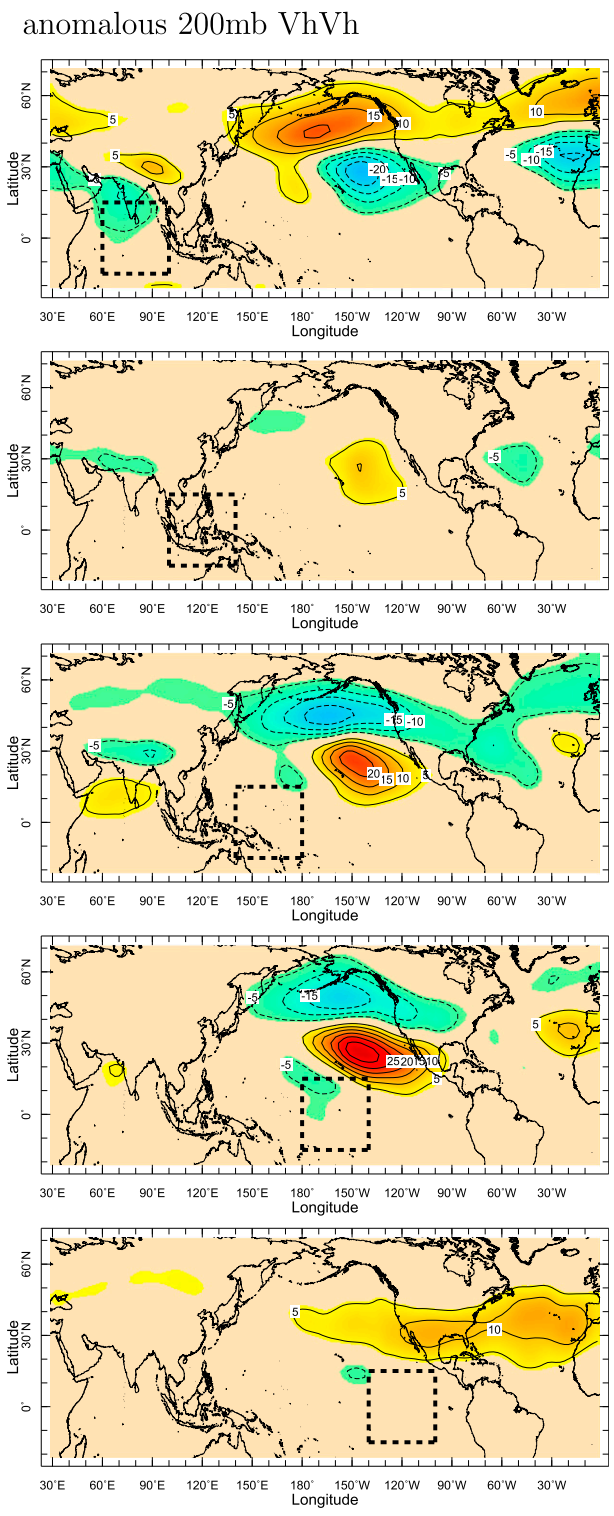

FIG. 5. The high-pass-filtered 200-mb meridional velocity variance ($m^2 s^{-2}$) for the box-SST anomaly experiments. The SST anomalies are shown in Fig. 3 and their location indicated here by the boxes. The meridional velocity variances were averaged over days 40–100 of 100-day simulations initiated on 1 December.

these responses are already establishing the west coast ridge. A weaker response to Indian Ocean SST anomalies is also apparent. The wave trains lead to intensification of the west coast ridge over the subsequent week. In tandem with the wave trains, the weaker eddy activity over the midlatitude eastern North Pacific Ocean and the United States and Mexico begins to be established by day 8 and also intensifies with the height anomalies over the subsequent week. The eddy weakening occurs where there are local easterly anomalies at 200 mb (deduced from the height anomalies) and the strengthening where anomalies are westward. This relation is consistent with changes in transient eddy propagation paths responding to the changes in the mean flow as in Seager et al. (2010b) and is qualitatively similar to that observed (Fig. 1).

6. The dynamical balance within the mean and transient circulation anomalies of winter 2013/14

a. The quasi-equilibrium vorticity balance in reanalysis and model simulation

How did the atmosphere achieve a seasonal mean state during winter 2013/14 that included such strong departures from the normal state? To examine this we turn to the upper-troposphere monthly mean vorticity budget, which can be written as

$$\frac{\partial \hat{\zeta}}{\partial t} + \hat{\mathbf{u}} \cdot \nabla \hat{\zeta} + \beta \hat{v} = -(\hat{\zeta} + f)\nabla \cdot \hat{\mathbf{u}} - \nabla \cdot (\widehat{\mathbf{u}''\zeta''}) + \hat{F}, \qquad (3)$$

where the hats denote monthly means and the double primes departures therefrom; ζ is relative vorticity; $\mathbf{u}$ is the horizontal vector velocity; f is the Coriolis parameter and β its meridional gradient; v is meridional velocity; F includes friction, diffusion, and the residual imbalance; and t is time. Terms involving vertical advection of vorticity, which tend to be small, have been neglected.

A common way to diagnose forcing of Rossby waves by tropical heating anomalies is to separate the anomalous flow into its rotational component, denoted by subscript ψ, and divergent component, denoted by subscript χ (i.e., $\hat{\mathbf{u}} = \hat{\mathbf{u}}_\psi + \hat{\mathbf{u}}_\chi$). Using this, and denoting anomalies by a single prime and climatological values by an overbar, e.g., $\hat{u} = \hat{u}' + \widehat{\overline{u}}$, the anomaly vorticity equation can be rewritten as

$$\begin{aligned} &\frac{\partial \widehat{\zeta'}}{\partial t} + \hat{\mathbf{u}}'_\psi \cdot \nabla \widehat{\overline{\zeta}} + (\widehat{\overline{\mathbf{u}}}_\psi \cdot \nabla \hat{\zeta}' + \beta \hat{v}'_\psi) \\ &\quad = -(\widehat{\overline{\zeta}} + f)\nabla \cdot \hat{\mathbf{u}}'_\chi - \hat{\zeta}' \nabla \cdot \widehat{\overline{\mathbf{u}}}_\chi - \beta \hat{v}'_\chi - \widehat{\overline{\mathbf{u}}}_\chi \cdot \nabla \hat{\zeta}' \\ &\qquad - \hat{\mathbf{u}}'_\chi \cdot \nabla \widehat{\overline{\zeta}} - \nabla \cdot (\widehat{\mathbf{u}''\zeta''})' + \hat{F}'. \end{aligned} \qquad (4)$$

These terms were computed for observations from the NCEP–NCAR reanalysis and ERA-Interim averaged

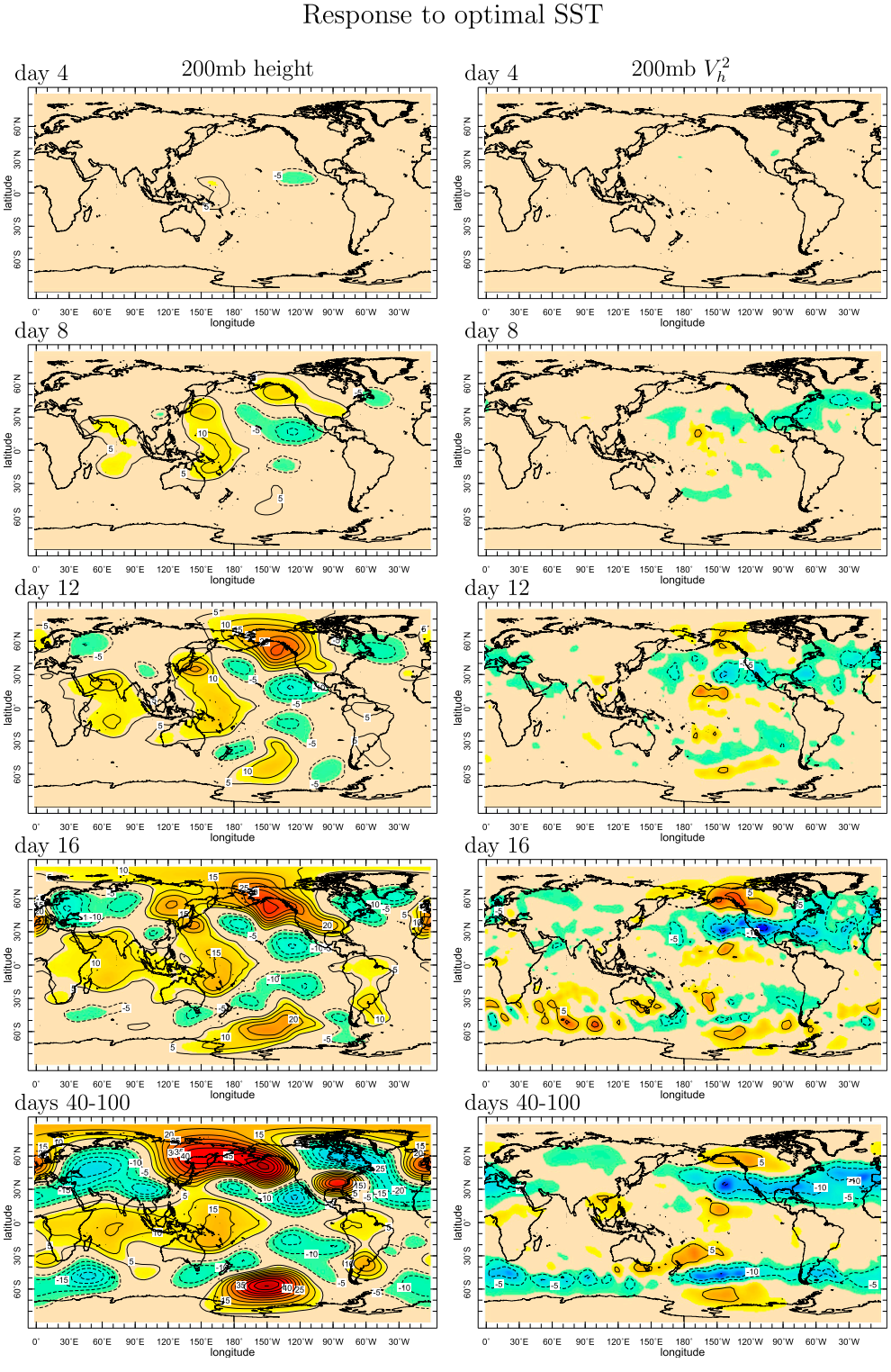

FIG. 6. The (left) 200-mb height anomaly (m) and (right) high-pass-filtered 200-mb meridional velocity variance ($m^2\,s^{-2}$) for responses to the optimal SST anomaly at different times following the switching on of the anomaly.

over DJF 2013/14 with anomalies defined as relative to a January 1979–April 2014 climatology. The results for both reanalyses were found to be very similar and here we show just the results from the NCEP–NCAR reanalysis since these were obtained at a spatial resolution more akin to that of the model simulations. The right-hand side of Eq. (4), minus the damping term, is referred to as the Rossby wave source [RWS; Sardeshmukh and Hoskins 1988; see also Trenberth et al. (1998), who use somewhat different notation]. Watson et al. (2016) show the RWS from ERA-Interim for the western Pacific domain and separate it into divergent and advection terms and their results are very similar to those shown here from the NCEP–NCAR reanalysis, but we continue by breaking the term down into its constituent parts to afford a more detailed process understanding. It was found that $\partial\hat{\zeta}'/\partial t$, $\hat{\zeta}'\nabla\cdot\widehat{\mathbf{u}}_\chi$, and $\widehat{\mathbf{u}}_\chi\cdot\nabla\hat{\zeta}'$ were sufficiently smaller than the other terms so they could be neglected in understanding the vorticity balances and its establishment. The term $\hat{\mathbf{u}}'_\chi\cdot\nabla\widehat{\zeta}$ is also small but is retained since this term has been appealed to as an important forcing in prior literature. Written in this way the rotational flow, as described by the left-hand side of Eq. (4), can be understood as a response to forcing involving the divergent flow on the right-hand side. The planetary vorticity advection and the advection of anomalous vorticity by the mean flow extensively balance each other as expected within a stationary barotropic Rossby wave and are grouped together ($\widehat{\mathbf{u}}_\psi\cdot\nabla\hat{\zeta}'+\beta\hat{v}'_\psi$) to allow better seeing the smaller imbalance that allows vertical motion. The six larger remaining terms from Eq. (4) are shown in Fig. 7.

The vorticity balance anomalies are seen to occur as part of waves of anomalies that stretch to North America from the Indian and tropical Pacific Ocean regions. Across the eastern Pacific and North America there is a balancing relationship between, on the one hand, the sum of mean flow advection of the vorticity anomalies and advection of the planetary vorticity by the rotational meridional wind anomaly [$(\widehat{\mathbf{u}}_\psi\cdot\nabla\hat{\zeta}'+\beta\hat{v}'_\psi)$, Fig. 7b] and, on the other hand, upper-tropospheric convergence and vortex compression [$-(\widehat{\zeta}+f)\nabla\cdot\hat{\mathbf{u}}'_\chi$, Fig. 7e]. The upper-troposphere convergence induces subsidence (not shown) at the west coast of North America, which would suppress precipitation, consistent with drought conditions. In contrast to the balance over the eastern Pacific–North America sector, over the Indian Ocean and western Pacific sectors the advection of the mean relative vorticity by the rotational flow anomalies (Fig. 7a), dominated by $\hat{v}'\partial\widehat{\zeta}/\partial y$, is important. This term sets up an east–west varying pattern that reflects the zonal variation in meridional flow anomalies that arises from the circulation responses to the multiple SST and convection anomalies in the tropics. These flow anomalies are located in a region of strong zonally uniform meridional gradient of mean relative vorticity (not shown) giving rise to this complex pattern.

The mechanism of establishment of the forcing for the Rossby waves differs somewhat from classical thinking (Sardeshmukh and Hoskins 1988; Trenberth et al. 1998) in that, across Asia and the subtropical western Pacific, the advection of mean relative vorticity by the anomalous divergent flow is much smaller than that by the rotational flow. Hence we do not have a clean separation with the rotational flow evolving in response to changes in the divergent flow. Instead the forced rotational flow interacts with the mean flow to cause a further evolution of the rotational flow anomaly.

The vorticity budget terms were also averaged over the last 60 days of the optimal SST forcing simulations. Anomalies in this case are the difference between the SST perturbed and unperturbed ensemble means. It was found that the terms that were small in the reanalysis were also small in the model and the same six larger terms in the model are shown in Fig. 8. The relative importance of the terms in the vorticity budget is very similar between the models and the reanalysis. The one exception is the much smoother transient eddy vorticity convergence in the model than the reanalysis, which simply comes about from the averaging across a 100-member ensemble compared to the single realization in nature. The individual terms in the vorticity balance also bear some similarity between model and reanalysis. Over western North America the model agrees with the observations that the upper-troposphere convergence (and, hence, subsidence below) arises from a three-way balance of vortex stretching, advection of planetary vorticity by the rotational meridional velocity anomaly, and advection by the mean flow of the vorticity anomaly (Fig. 8b). The model agrees that advection of the mean relative vorticity by the rotational flow (Fig. 8a) dominates over that by the divergent flow (Fig. 8c). Similarly this sets up in the model a zonally varying, meridionally confined, anomalous vorticity tendency over South Asia and the subtropical western Pacific. The locations of the features within this term, however, do not agree between the model and reanalysis, which could be due to model bias in the location of the tropical heating, in the flow response, or in the mean state, which allows a phase error in the wave response.

The transient eddy vorticity flux convergence term (Fig. 8f) is not small. However, it also does not appear to systematically contribute to the maintenance of the

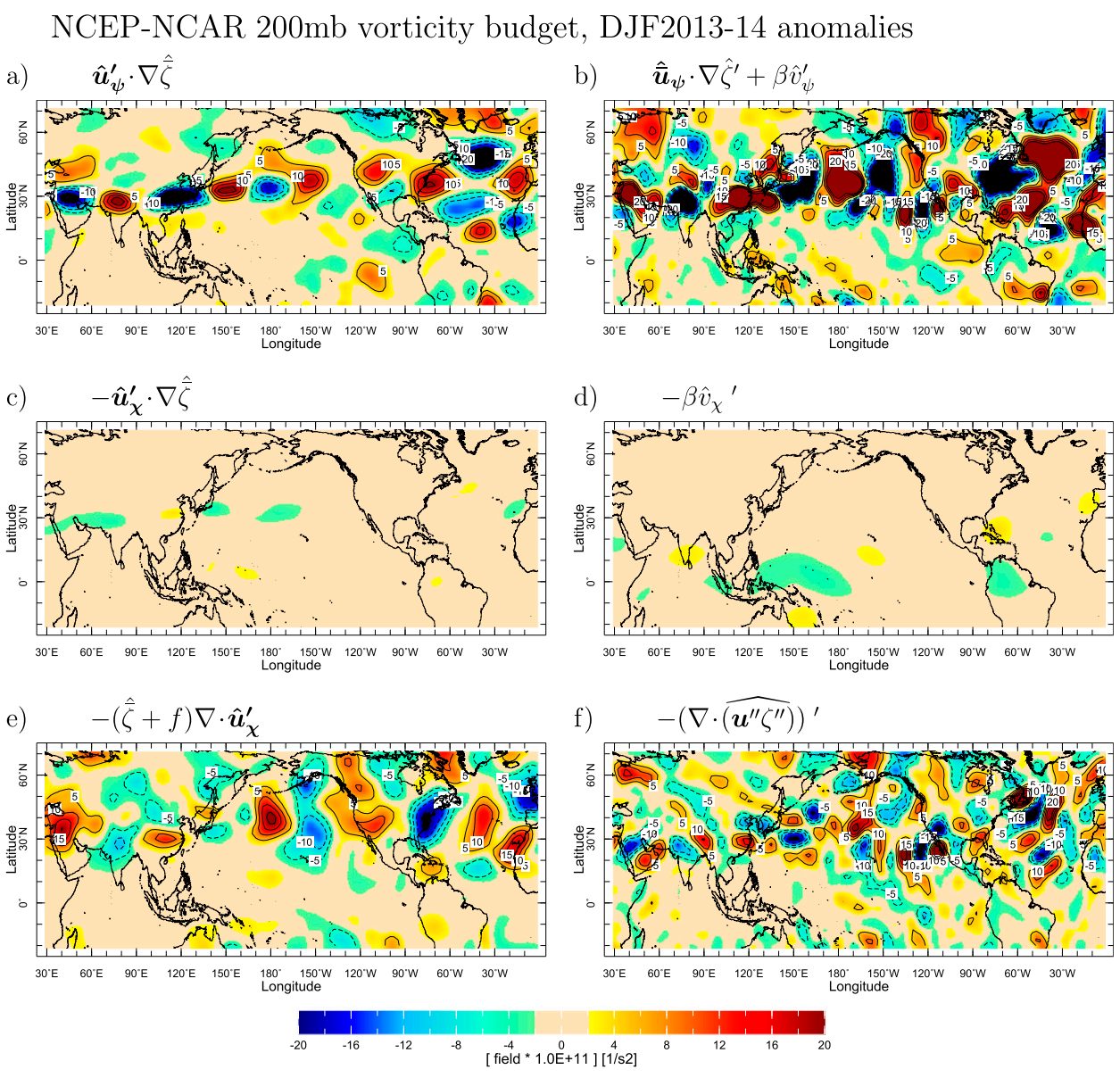

FIG. 7. The terms in the 200-mb vorticity (s^{-2}) budget from the NCEP–NCAR reanalysis averaged over DJF 2013/14. Units for the terms have been multiplied by 10^{11} for plotting purposes.

large-scale circulation anomaly pattern being instead rather noisy. This is in contrast to the results of Seager et al. (2003, 2010b) and Harnik et al. (2010), who found that transient eddy momentum fluxes were important to developing and sustaining mean flow anomalies during El Niño events, but the results are not necessarily inconsistent. The earlier results concerned El Niño events, which could have a different eddy–mean flow interaction process to that occurring during winter 2013/14 and its model analog. Also the earlier results made much of the case for a positive eddy–mean flow feedback by analyzing longitudinally averaged quantities whereas here our focus is on explaining the west coast ridge of winter 2013/14, a very longitudinally localized feature.

b. *Observed and modeled tropical forcing of circulation anomalies*

Copsey et al. (2006) point out that imposing SST anomalies over the Indian Ocean can lead in a model to wrong sign precipitation and surface pressure responses. An incorrect response would also be apparent in the divergent wind response to the SST and precipitation anomalies. Since our arguments to date rely heavily on an SST-forced model, and the optimal SST methodology

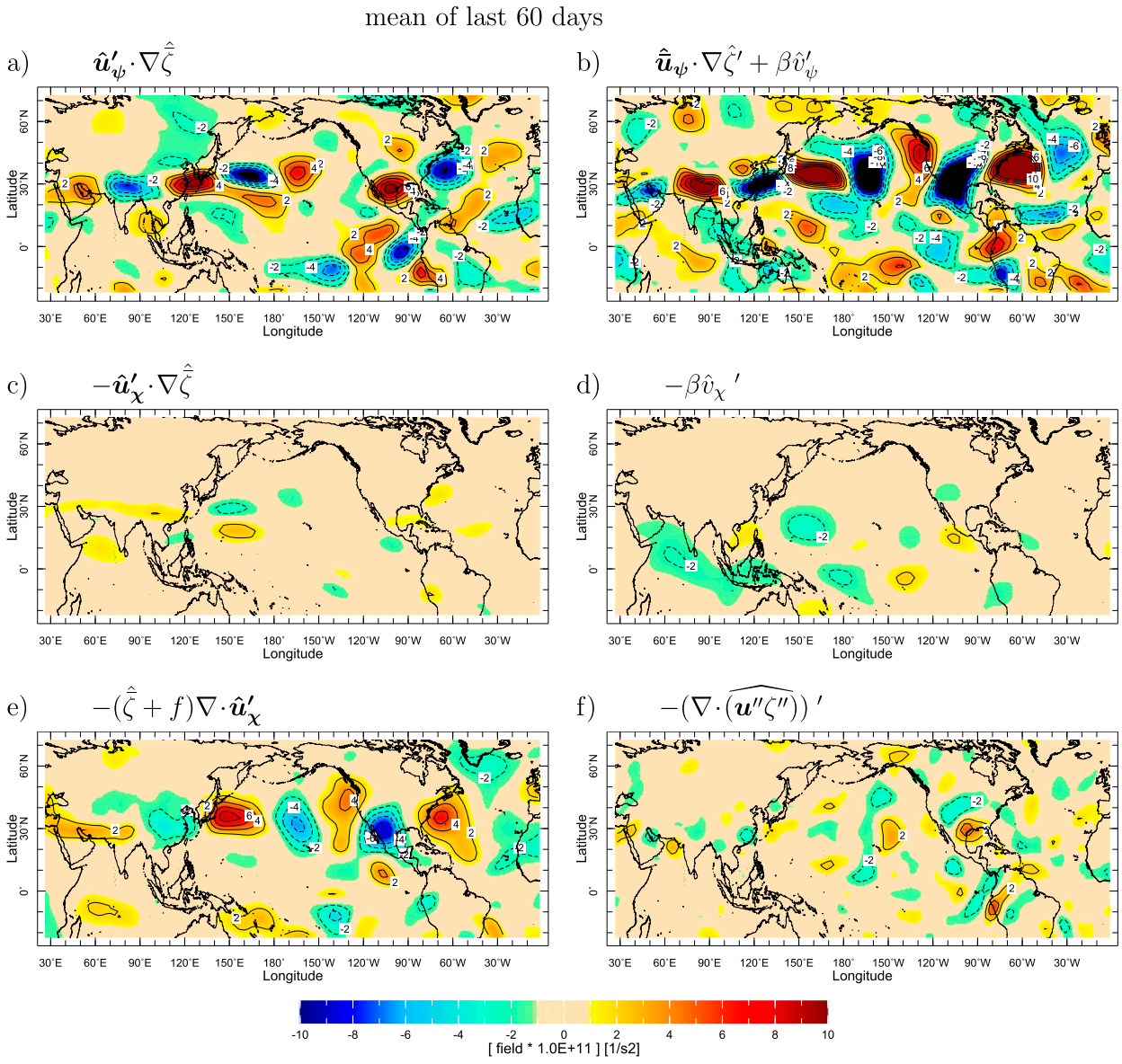

FIG. 8. As in Fig. 7, but for the 100-member ensemble mean of the last 60 days of the model simulations of the response to the optimal SST pattern.

allows this error to occur, in Fig. 9 we show the DJF 2013/14 anomalies of surface pressure over the ocean and 200-mb divergent wind and velocity potential (Φ', related as $\hat{\mathbf{u}}'_{\chi}=\nabla\hat{\Phi}'$) from the NCEP–NCAR reanalysis and averaged over the last 60 days of the model simulations of the response to the optimal SST pattern. The upper-troposphere divergence anomalies over the western tropical Pacific are striking in both observations and model. The model has a weaker divergence center over the Indian Ocean and a convergence center over Southeast Asia, which is barely present in observations. The model correctly reproduces the low surface pressure anomaly across the Indian Ocean and western tropical Pacific and high anomalies in the central (observations) and eastern (model) tropical Pacific. The comparison suggests that the model response is more realistic over the Pacific sector of the tropics than the Indian Ocean sector. This is reassuring as the optimization invokes SST anomalies that are greater over the Pacific than the Indian Ocean. Further much of the wave forcing is by the rotational as opposed to

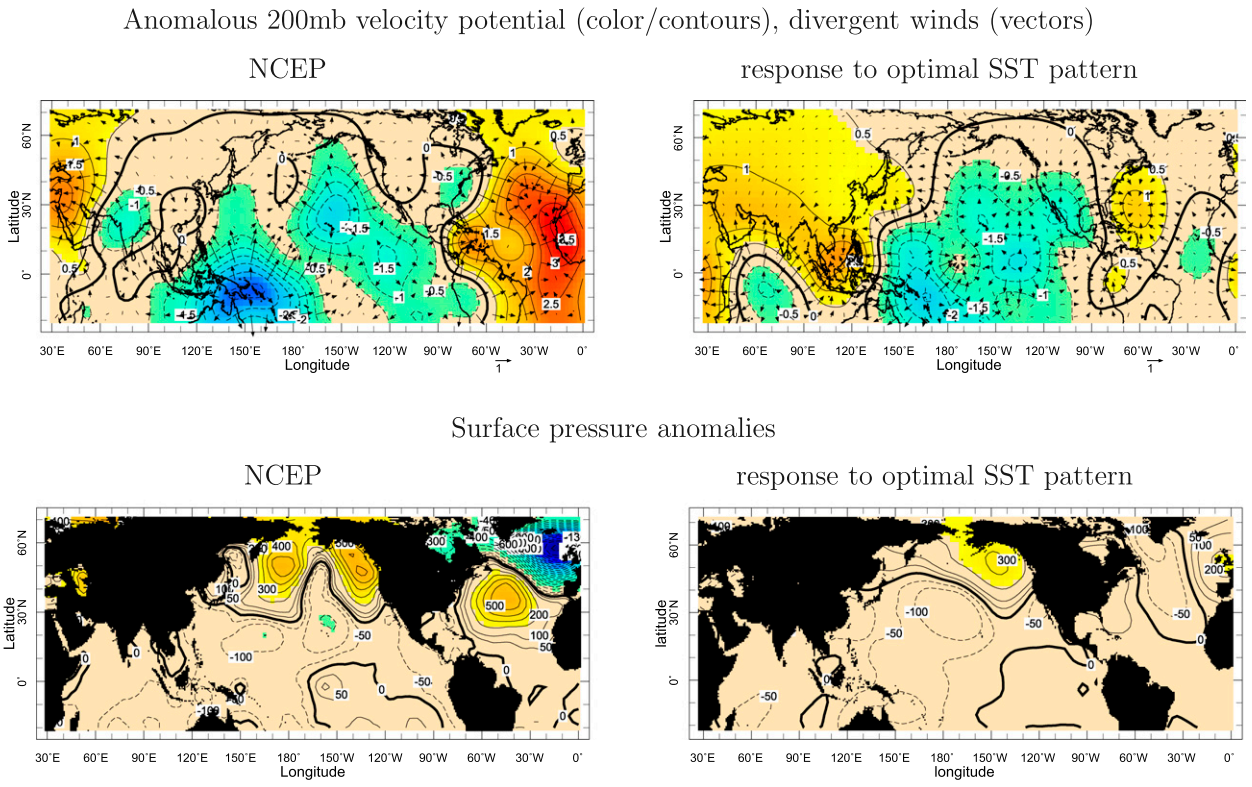

FIG. 9. (left) The NCEP–NCAR reanalysis winter 2013/14 and (right) 100-member ensemble mean of the last 60 days of the model simulations of the response to the optimal SST pattern, showing (top) anomalous divergent wind ($m\,s^{-1}$) and velocity potential (s^{-1}, multiplied by 10^6) and (bottom) anomalous surface pressure over ocean (Pa).

divergent flow, although these components will be related. However, this comparison provides some additional confidence that the model results provide information on the potential role of the tropical SST anomalies in generating the west coast ridge of winter 2013/14. (Agreement is poor over the Atlantic, consistent with little evidence that circulation anomalies there were forced from the Indian and Pacific Oceans.)

c. *The transient evolution of the vorticity balance in the model simulation*

It is not possible to establish cause and effect in the establishment of the vorticity balance in the reanalysis because the atmosphere is always in a statistical equilibrium with the slowly evolving SST anomalies. As in Fig. 6 for the height field and storm track, here we examine how the vorticity budget evolves on a day-by-day and weekly basis. Results are shown in Fig. 10 for the leading terms in the vorticity budget given by

$$\mathbf{u}'_{\psi}\cdot\nabla\overline{\zeta}+\overline{\mathbf{u}}_{\psi}\cdot\nabla\zeta'+\beta v'_{\psi}=-f\nabla\cdot\mathbf{u}'_{\chi}. \qquad (5)$$

Here the anomalies and climatology are both on the daily time scale with the anomalies defined as the difference between the SST-perturbed and control ensemble means. Early on at day 5 there are various vorticity tendency terms related to the advection of the mean relative vorticity gradient by the anomalous rotational flow across the tropical Pacific north of the equator. This term is dominated by its meridional component $\hat{v}'_{\psi}\widehat{\overline{\zeta}}_{y}$ (not shown). This entire term has grown by day 11 and is being balanced in large part by the sum of mean flow advection of the relative vorticity anomaly and the anomalous advection of planetary vorticity and to a lesser extent by the term involving the upper-troposphere divergence anomaly. The latter convergence over the west coast of North America that, by mass continuity, will require subsidence below, is only barely evident by day 17 but intensifies over subsequent weeks. Further examination shows that, over the western Pacific, the advection of mean relative vorticity by the anomalous rotational flow is dominated by the meridional flow anomaly but in the eastern Pacific–North America sector the advection by anomalous zonal flow is the leading term. The vorticity balance terms intensify to day 17 but the balance among the terms remains essentially the same.

This can be understood in terms of the transient evolution of the flow anomaly field ($\hat{u}'_{\psi}$, $\hat{u}'_{\chi}$, $\hat{v}'_{\psi}$, and $\hat{v}'_{\chi}$),

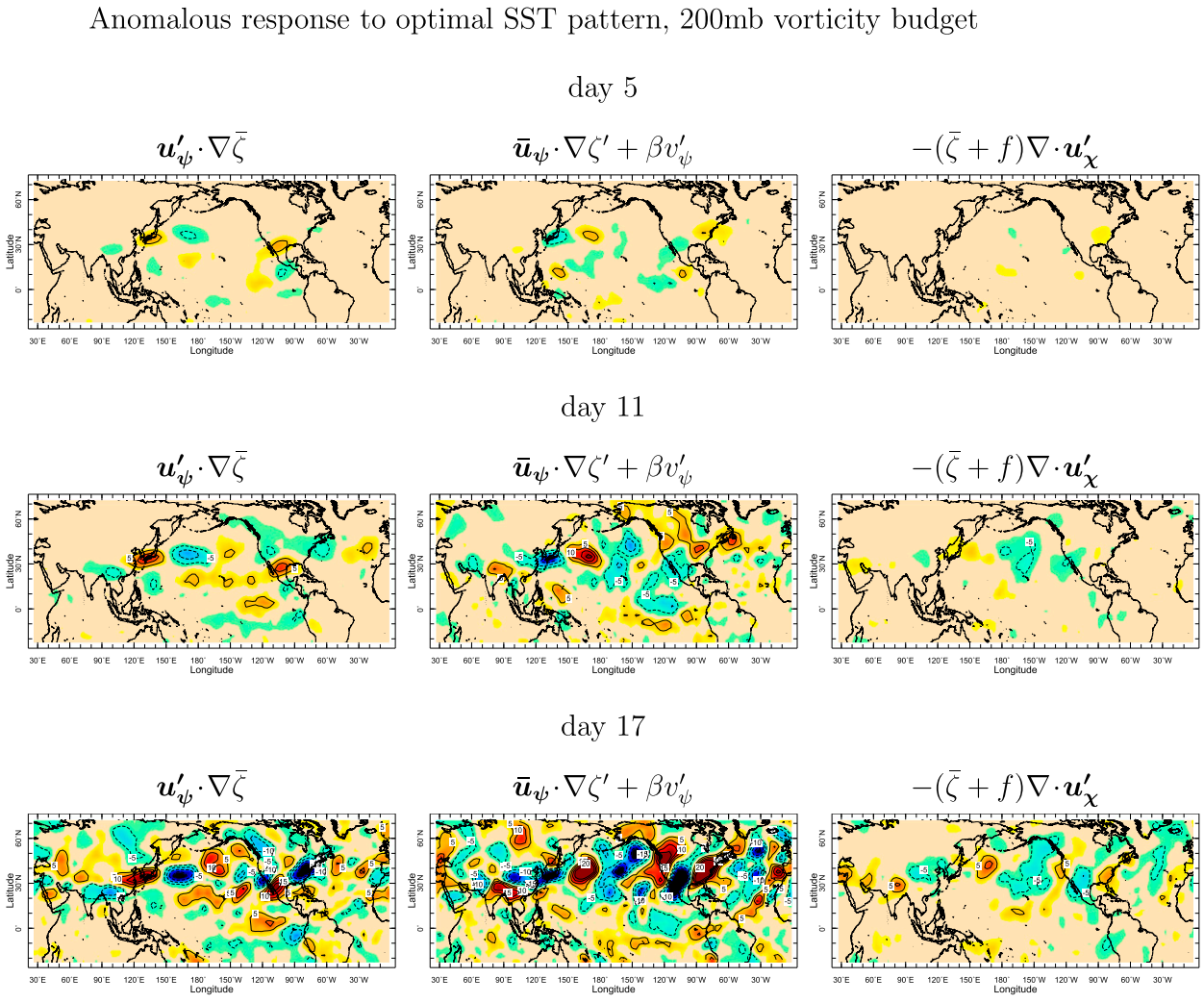

FIG. 10. (top) Day 5, (middle) day 11, and (bottom) day 17 snapshots of the transient evolution of (left)–(right) the leading terms in the vorticity budget of the 100-member ensemble mean of the optimal SST anomaly switch-on experiments (s^{-2}). Units for the terms have been multiplied by 10^{11} for plotting purposes.

as shown in Fig. 11. The warm SST and positive precipitation anomaly over the western Pacific Ocean excites local upper-troposphere off-equatorial anticyclonic anomalies to the west and equatorial westerly and cyclonic anomalies to the east. The latter are clearer because the heating forced response to the west is in a location where there will also be responses to the SST anomalies over the Maritime Continent region and Indian Ocean. Looking at the transition from day 5 to day 11, the cyclonic anomaly over the eastern Pacific is now at the root of a wave train that has propagated northeastward and placed easterly anomalies at the west coasts of the United States and Mexico. In addition a wave easily seen in the meridional flow field has propagated from the northern Indian Ocean–South Asian–tropical western Pacific region eastward across the Pacific and placed northerly flow at the west coast centered on the Canadian–U.S. border region. The vorticity balance that is established therefore arises from a combination of these wave fields originating across the Indo-Pacific region but with the end result of high pressure and subsidence at the west coast of North America that would act to suppress precipitation.

7. Explaining the west coast ridge of winter 2013/14 in terms of SST forcing plus internal atmospheric variability

The modeling results presented, and those by others (e.g., Watson et al. 2016), do not support the idea that the full amplitude of the west coast ridge of winter 2013/14 was SST forced. Instead it is argued that the full

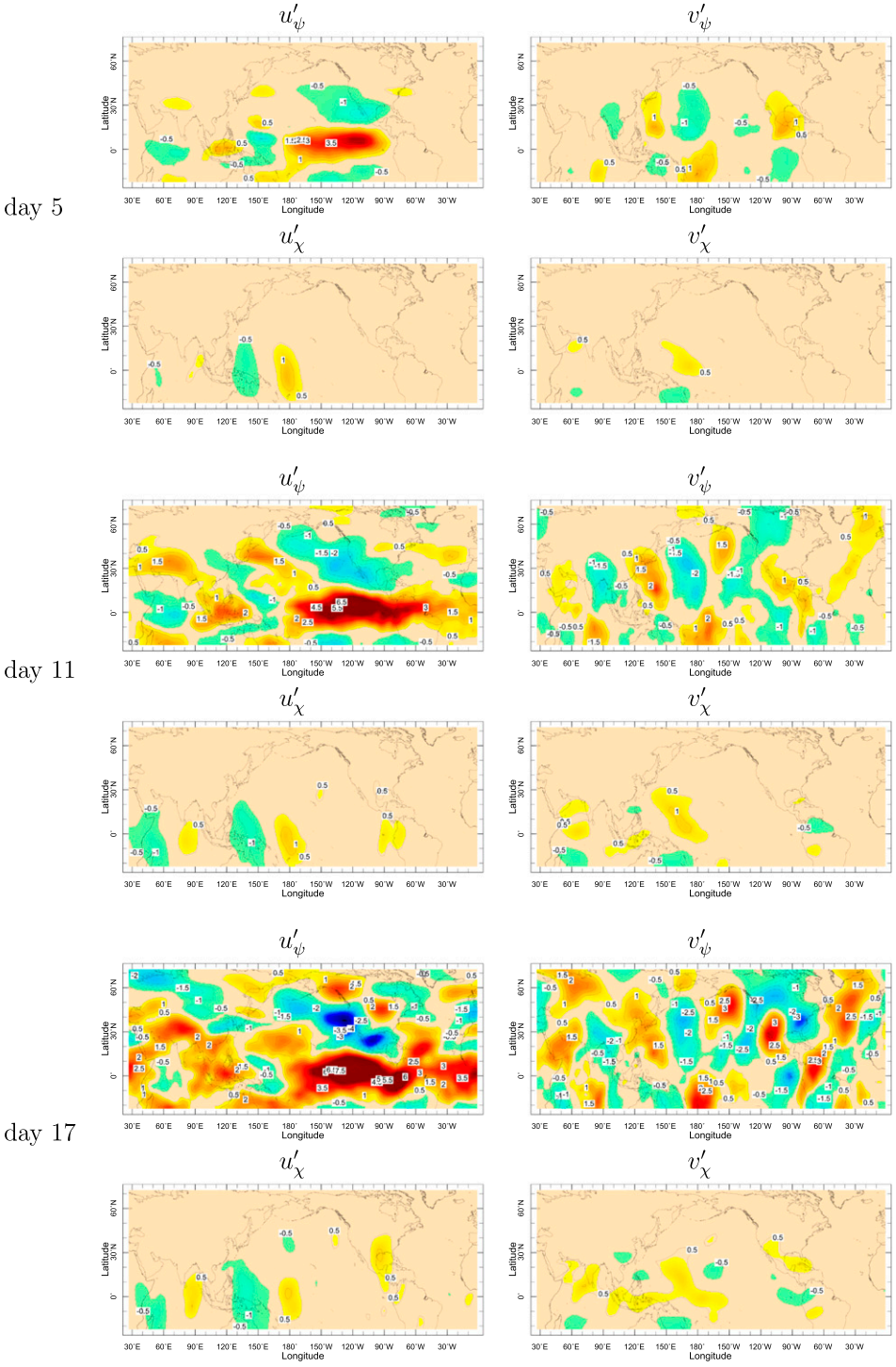

FIG. 11. As in Fig. 10, but for the rotational and divergent components of the (left) zonal and (right) meridional flow anomalies ($\mathrm{m\,s^{-1}}$). For plotting purposes contours and colors corresponding to more than $\pm 5\,\mathrm{m\,s^{-1}}$ are not shown.

amplitude is explained by a combination of an SST-forced response and internal atmospheric variability acting constructively. Given that we have ensembles with 100 members that can span a wide, if not complete, range of internal atmosphere variability, it is worth examining if some ensemble members have a ridge amplitude as large as that observed. To determine this we computed the pattern correlation between the observed DJF 2013/14 200-mb height anomaly and that of the ensemble members in the simulation forced by the optimal SST pattern, with the anomaly defined as the difference between the ensemble member and the 100-member mean of the control ensemble with unperturbed SSTs. Figure 12 plots the height and precipitation anomalies of the four ensemble members with the highest correlation. It is possible to get a height anomaly very similar in pattern (including the Hudson Bay trough) and magnitude to that observed. Notably these ensemble members also had tropical precipitation anomalies akin to the ensemble mean and the observations. We also performed the same calculation using the 100 control ensemble members with anomalies defined as relative to the ensemble mean and found that, even without anomalous SST forcing, some ensemble members could produce a west coast ridge akin in pattern and magnitude to that observed. Figure 12 also, therefore, shows histograms of the pattern correlations for the two 100-member ensembles. While both ensembles essentially span from -1 to 1, the SST-forced ensemble, relative to the unperturbed ensemble, is clearly shifted toward more positive values. The two distributions are significantly different, according to the Kolmogorov–Smirnov test, with greater than 99% confidence. This result illustrates how internal atmospheric variability could alone create height anomalies akin to the one observed but that the presence of the Indo-Pacific SST anomalies made the observed height anomaly considerably more probable. For example, the presence of the SST forcing made anomalies that matched the observed with a pattern correlation of 0.6 or more 3 times more likely than without the SST anomalies.

8. Conclusions and discussion

We have investigated the dynamical causes of the North American west coast ridge of winter 2013/14 that caused the driest winter during the recent California drought and examined the role in generating it of SST anomalies in the tropical Pacific and Indian Oceans. Conclusions are as follows:

- Prior work has suggested the drought-inducing North American west coast ridge of winter 2013/14 was partly forced by SST anomalies. However different SST datasets disagree on the amplitude and to some extent the pattern of the SST anomalies with the result that the same atmosphere model forced by the different SST datasets simulates the ridge with different levels of realism.
- Motivated by the uncertainty in regard to the SST anomalies that were actually present in winter 2013/14, we adopted a ''constructive modeling'' approach and found an optimal pattern of tropical Indo-Pacific SST anomalies that produced a model response that best matched the observed Northern Hemisphere height anomaly in DJF 2013/14. A pattern with a warm SST anomaly in the western Pacific, cool in the central Pacific, near neutral values in the Maritime Continent region, and a weak warm anomaly in the Indian Ocean produces a height response that provides the best match including a west coast ridge. The height response can be understood as a linear combination of waves forced by the individual anomalies. Despite the optimization methodology, the modeled ridge is considerably weaker than that observed, lending support to the idea that SST forcing played a limited, if important, role in generating the ridge.
- In both observations for DJF 2013/14 and the optimal forcing simulations the west coast ridge is also associated with suppression of storm-track activity with increased activity toward the north and south. This rearrangement of transient eddy activity, which essentially acts to shield California from moisture-laden storms, would have aided in generating drought conditions.
- The fundamental features of the vorticity balance within the circulation anomaly are associated with the mean flow terms involving advection of the mean relative vorticity field by the rotational flow, advection of the relative vorticity anomaly by the mean zonal flow, the anomalous planetary vorticity advection, and vortex stretching. It is vortex compression over the west coast that will act to induce subsidence and also suppress precipitation. We do not find clear evidence of a feedback between the eddy vorticity fluxes and the mean flow.
- The transient day-by-day and week-by-week evolution of the model response to the optimal SST forcing shows that the collection of tropical SST anomalies generate upper-troposphere rotational flow anomalies that create anomalous advection of mean relative and planetary vorticity and force Rossby waves to propagate and within days reach the west coast of North America establishing the ridge by the vorticity balance described above. As the mean flow circulation anomaly develops so does the reduction in eddy

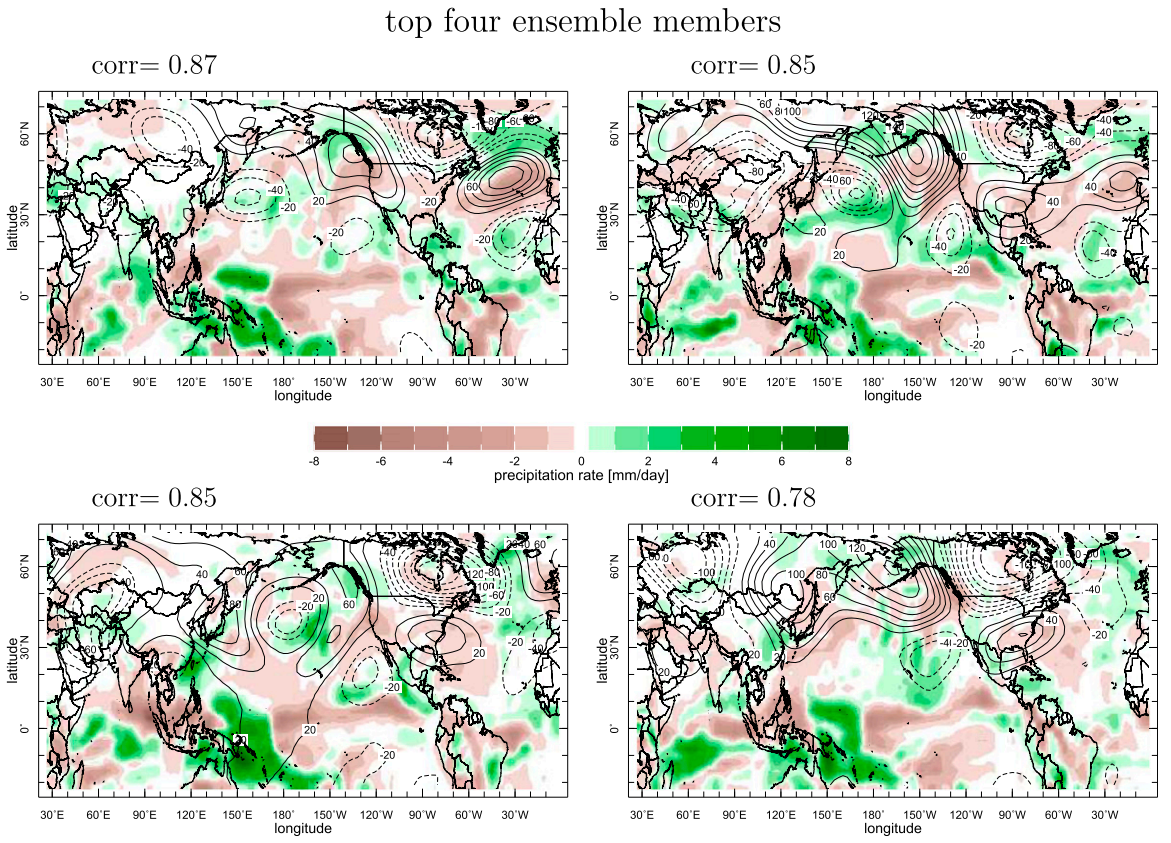

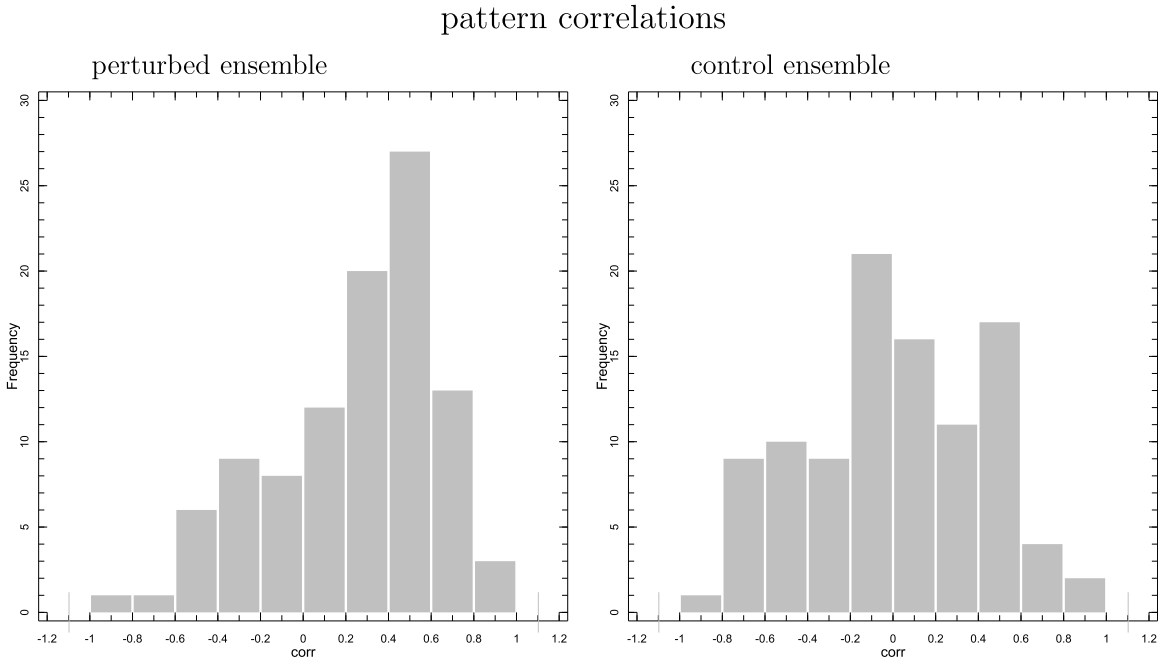

FIG. 12. (top),(middle) The 200-mb height (contours; m) and precipitation (color; mm day^{-1}) anomaly for the four optimal SST anomaly perturbed ensemble members that have the highest extratropical pattern correlation with the observed DJF 2013/14 height anomaly. (bottom) Histograms of pattern correlation coefficients between the extratropical height anomalies of the ensemble members and the observed DJF 2013/14 anomaly for (left) the control ensemble and (right) the optimized SST anomaly perturbed ensemble.

activity over the western Pacific and North America at the latitude of the United States and Mexico.
- A combination of SST-forced response and internal atmosphere variability can provide a reasonable match to the observed height anomaly in terms of pattern and amplitude. The presence of SST forcing notably increases the probability of such a height anomaly occurring.

To conclude, the work presented here is highly suggestive that tropical Indo-Pacific SST anomalies and associated precipitation anomalies forced a collection of Rossby wave responses that in sum contributed to the unusual North American west coast ridge of winter 2013/14. Hence, we argue, that the ridge depended on a more general anomalous tropical ocean state than just the warm western tropical Pacific whose impacts were focused on by Watson et al. (2016). The results are, however, not conclusive largely because the actual SST anomalies during this winter are not known to the level of accuracy that is apparently needed to successfully reproduce in models the correct atmospheric response. Hence it remains uncertain exactly what SST anomalies were responsible and also whether there was an additional role in the wave forcing for precipitation anomalies that were not tied to the underlying SSTs. A clear avenue for future research must be to determine why different state-of-the-art SST datasets differ to the degree they do in the modern era of quite abundant observational data. A second avenue for research should be to determine what caused the drought-forcing SST anomalies and how well they, and the atmospheric response to them, can be forecast. The results indicate that they were driven by anomalous ocean heat flux convergence but the causes of that are unknown. It would be interesting to identify the wind forcing and changes in currents, mixing and thermocline depth responsible and to also determine if these arise as an occasional part of the ENSO cycle or are a different phenomenon, or are influenced by human-driven climate change.

The results presented here suggest processes additional to tropical SST forcing were also involved in generating the west coast ridge, including internal atmosphere variability as argued by Seager et al. (2015), Baxter and Nigam (2015), and Watson et al. (2016) or forcing from other changes in ocean surface conditions (Lee et al. 2015). In terms of any role for climate change it should be noted that the current work indicates that a key feature of the SST anomaly for generating the ridge was warming in the western Pacific relative to the more eastern part of the ocean. That is why Palmer (2014) noted that for anthropogenic climate change to have played a role in the SST states that contributed to the extreme winter of 2013/14 it would require a nonuniform SST response to radiative forcing and essentially invoked the ocean dynamical thermostat mechanism of Clement et al. (1996) and Cane et al. (1997). Whether such a dynamically forced SST change is occurring in nature is unknown but needs to be determined. Whatever the answer, the fact that tropical SST anomalies, which are from neither El Niño nor La Niña, can help create such a dramatic climate anomaly over North America as the west coast ridge of winter 2013/14 is interesting and, now that it is identified, should provide a means to improve seasonal prediction for the continent provided that the SST anomalies can, first, be monitored with sufficient accuracy and, second, predicted.

Acknowledgments. This work was supported by NSF Awards AGS-1401400 and AGS-1243204, NOAA Award NA14OAR4310232, and, in part, by WSL PURE in partnership with Columbia University's Center for Climate and Life. We thank Mark Cane and Dong-Eun Lee for conversations and additional simulations analyzing sensitivity of circulation anomalies to SST datasets. We also thank three anonymous reviewers for constructive criticism.

REFERENCES

Adler, R. F., and Coauthors, 2003: The version-2 Global Precipitation Climatology Project (GPCP) monthly precipitation analysis (1979–present). *J. Hydrometeor.*, **4**, 1147–1167, doi:10.1175/1525-7541(2003)004<1147:TVGPCP>2.0.CO;2.

Alexander, M. A., 1992a: Midlatitude atmosphere–ocean interaction during El Niño. Part I: The North Pacific Ocean. *J. Climate*, **5**, 944–958, doi:10.1175/1520-0442(1992)005<0944:MAIDEN>2.0.CO;2.

——, 1992b: Midlatitude atmosphere–ocean interaction during El Niño. Part II: The Northern Hemisphere. *J. Climate*, **5**, 959–972, doi:10.1175/1520-0442(1992)005<0959:MAIDEN>2.0.CO;2.

Balmaseda, M. A., K. Mogensen, and A. T. Weaver, 2013: Evaluation of the ECMWF Ocean Reanalysis System ORAS4. *Quart. J. Roy. Meteor. Soc.*, **139**, 1132–1161, doi:10.1002/qj.2063.

Baxter, S., and S. Nigam, 2015: Key role of the North Pacific Oscillation–west Pacific pattern in generating the extreme 2013/14 North American winter. *J. Climate*, **28**, 8109–8117, doi:10.1175/JCLI-D-14-00726.1.

Berrisford, P., P. Kallberg, S. Kobayashi, D. Dee, S. Uppala, A. J. Simmons, P. Poli, and H. Sato, 2011a: Atmospheric conservation properties in ERA-Interim. *Quart. J. Roy. Meteor. Soc.*, **137**, 1381–1399, doi:10.1002/qj.864.

——, and Coauthors, 2011b: The ERA-Interim archive version 2.0. ERA Rep. Series 1, 23 pp. [Available online at http://www.ecmwf.int/en/elibrary/8174-era-interim-archive-version-20.]

Bond, N. E., M. F. Cronin, H. Freeland, and N. Mantua, 2015: Causes and impacts of the 2014 warm anomaly in the NE Pacific. *Geophys. Res. Lett.*, **42**, 3414–3420, doi:10.1002/2015GL063306.

Cane, M. A., A. C. Clement, A. Kaplan, Y. Kushnir, D. Pozdnyakov, R. Seager, S. E. Zebiak, and R. Murtugudde, 1997: Twentieth-century sea surface temperature trends. *Science*, **275**, 957–960, doi:10.1126/science.275.5302.957.

Cayan, D., 1992: Latent and sensible heat flux anomalies over the northern oceans: Driving the sea surface temperature. *J. Phys. Oceanogr.*, **22**, 859–881, doi:10.1175/1520-0485(1992)022<0859:LASHFA>2.0.CO;2.

Clement, A. C., R. Seager, M. A. Cane, and S. E. Zebiak, 1996: An ocean dynamical thermostat. *J. Climate*, **9**, 2190–2196, doi:10.1175/1520-0442(1996)009<2190:AODT>2.0.CO;2.

Copsey, D., R. Sutton, and J. R. Knight, 2006: Recent trends in sea level pressure in the Indian Ocean region. *Geophys. Res. Lett.*, **33**, L19712, doi:10.1029/2006GL027175.

Davies, H. C., 2015: Weather chains during the 2013/14 winter and their significance for seasonal prediction. *Nat. Geosci.*, **8**, 833–837, doi:10.1038/ngeo2561.

Dee, D., and Coauthors, 2011: The ERA-Interim reanalysis: Configuration and performance of the data assimilation system. *Quart. J. Roy. Meteor. Soc.*, **137**, 553–597, doi:10.1002/qj.828.

Funk, C., A. Hoell, and D. Stone, 2014: Examining the contribution of the observed global warming trend to the California droughts of 2012/13 and 2013/14 [in "Explaining Extreme Events of 2013 from a Climate Perspective"]. *Bull. Amer. Meteor. Soc.*, **95** (9), S11–S15, doi:10.1175/1520-0477-95.9.S1.1.

Gill, A. E., 1980: Some simple solutions for heat induced tropical circulation. *Quart. J. Roy. Meteor. Soc.*, **106**, 447–462, doi:10.1002/qj.49710644905.

Harnik, N., R. Seager, N. Naik, M. Cane, and M. Ting, 2010: The role of linear wave refraction in the transient eddy–mean flow response to tropical Pacific SST anomalies. *Quart. J. Roy. Meteor. Soc.*, **136**, 2132–2146, doi:10.1002/qj.688.

Hartmann, D. L., 2015: Pacific sea surface temperature and the winter of 2014. *Geophys. Res. Lett.*, **42**, 1894–1902, doi:10.1002/2015GL063083.

Herring, S. C., M. P. Hoerling, T. C. Peterson, and P. A. Stott, 2014: Explaining extreme events of 2013 from a climate perspective. *Bull. Amer. Meteor. Soc.*, **95**, S1–S104, doi:10.1175/1520-0477-95.9.S1.1.

Hoerling, M. P., J. W. Hurrell, and T. Xu, 2001: Tropical origins for recent North Atlantic climate change. *Science*, **292**, 90–92, doi:10.1126/science.1058582.

Hoskins, B., and K. Karoly, 1981: The steady response of a spherical atmosphere to thermal and orographic forcing. *J. Atmos. Sci.*, **38**, 1179–1196, doi:10.1175/1520-0469(1981)038<1179:TSLROA>2.0.CO;2.

Howitt, R. E., J. Medellin-Azuara, D. MacEwan, J. R. Lund, and D. A. Summer, 2014: Economic analysis of the 2014 drought for California agriculture. Tech. Rep., Center for Watershed Sciences, University of California, Davis, 20 pp. [Available online at https://watershed.ucdavis.edu/2014-drought-report.]

Huang, B., and Coauthors, 2015: Extended Reconstructed Sea Surface Temperature version 4 (ERSST.v4). Part I: Upgrades and intercomparisons. *J. Climate*, **28**, 911–930, doi:10.1175/JCLI-D-14-00006.1.

Huffman, G. J., and Coauthors, 1997: The Global Precipitation Climatology Project (GPCP) combined precipitation dataset. *Bull. Amer. Meteor. Soc.*, **78**, 5–20, doi:10.1175/1520-0477(1997)078<0005:TGPCPG>2.0.CO;2.

Kiehl, J. T., J. J. Hack, G. B. Bonan, B. A. Bovile, D. L. Williamson, and P. J. Rasch, 1998: The National Center for Atmospheric Research Community Climate Model: CCM3. *J. Climate*, **11**, 1131–1149, doi:10.1175/1520-0442(1998)011<1131:TNCFAR>2.0.CO;2.

Kistler, R., and Coauthors, 2001: The NCEP–NCAR 50-Year Reanalysis: Monthly means CD-ROM and documentation. *Bull. Amer. Meteor. Soc.*, **82**, 247–268, doi:10.1175/1520-0477(2001)082<0247:TNNYRM>2.3.CO;2.

Lau, N.-C., and M. J. Nath, 1994: A modeling study of the relative roles of tropical and extratropical SST anomalies in the variability of the global atmosphere–ocean system. *J. Climate*, **7**, 1184–1207, doi:10.1175/1520-0442(1994)007<1184:AMSOTR>2.0.CO;2.

——, and ——, 1996: The role of the "atmospheric bridge" in linking tropical Pacific ENSO events to extratropical SST anomalies. *J. Climate*, **9**, 2036–2057, doi:10.1175/1520-0442(1996)009<2036:TROTBI>2.0.CO;2.

Lee, M., C. Hong, and H. Hsu, 2015: Compounding effects of warm sea surface temperature and reduced sea ice on the extreme circulation over the extratropical North Pacific and North America during the 2013-14 boreal winter. *Geophys. Res. Lett.*, **42**, 1612–1618, doi:10.1002/2014GL062956.

Palmer, T. N., 2014: Record breaking winters and global climate change. *Science*, **344**, 803–804, doi:10.1126/science.1255147.

Rayner, N., D. Parker, E. Horton, C. Folland, L. Alexander, D. Rowell, E. Kent, and A. Kaplan, 2003: Global analyses of sea surface temperature, sea ice, and night marine air temperature since the late nineteenth century. *J. Geophys. Res.*, **108**, 4407, doi:10.1029/2002JD002670.

Sardeshmukh, P. D., and B. J. Hoskins, 1988: The generation of global rotational flow by steady idealized tropical divergence. *J. Atmos. Sci.*, **45**, 1228–1251, doi:10.1175/1520-0469(1988)045<1228:TGOGRF>2.0.CO;2.

Seager, R., N. Harnik, Y. Kushnir, W. Robinson, and J. Miller, 2003: Mechanisms of hemispherically symmetric climate variability. *J. Climate*, **16**, 2960–2978, doi:10.1175/1520-0442(2003)016<2960:MOHSCV>2.0.CO;2.

——, Y. Kushnir, C. Herweijer, N. Naik, and J. Velez, 2005: Modeling of tropical forcing of persistent droughts and pluvials over western North America: 1856–2000. *J. Climate*, **18**, 4065–4088, doi:10.1175/JCLI3522.1.

——, and Coauthors, 2009: Mexican drought: An observational, modeling and tree ring study of variability and climate change. *Atmósfera*, **22**, 1–31.

——, N. Naik, W. Baethgen, A. Robertson, Y. Kushnir, J. Nakamura, and S. Jurburg, 2010a: Tropical oceanic causes of interannual to multidecadal precipitation variability in southeast South America over the past century. *J. Climate*, **23**, 5517–5539, doi:10.1175/2010JCLI3578.1.

——, ——, M. A. Cane, N. Harnik, M. Ting, and Y. Kushnir, 2010b: Adjustment of the atmospheric circulation to tropical Pacific SST anomalies: Variability of transient eddy propagation in the Pacific–North America sector. *Quart. J. Roy. Meteor. Soc.*, **136**, 277–296, doi:10.1002/qj.588.

——, L. Goddard, J. Nakamura, N. Naik, and D. E. Lee, 2014a: Dynamical causes of the 2010/11 Texas–northern Mexico drought. *J. Hydrometeor.*, **15**, 39–68, doi:10.1175/JHM-D-13-024.1.

——, D. Neelin, I. Simpson, H. Liu, N. Henderson, T. Shaw, Y. Kushnir, and M. Ting, 2014b: Dynamical and thermodynamical causes of large-scale changes in the hydrological cycle over North America in response to global warming. *J. Climate*, **27**, 7921–7948, doi:10.1175/JCLI-D-14-00153.1.

——, M. Hoerling, S. Schubert, H. Wang, B. Lyon, A. Kumar, J. Nakamura, and N. Henderson, 2015: Causes of the 2011–14 California drought. *J. Climate*, **28**, 6997–7024, doi:10.1175/JCLI-D-14-00860.1.

Swain, D., M. Tsiang, M. Haughen, D. Singh, A. Charland, B. Rajarthan, and N. S. Diffenbaugh, 2014: The extraordinary California drought of 2013/14: Character, context, and the role of climate change [in "Explaining Extreme Events of 2013 from

a Climate Perspective"]. *Bull. Amer. Meteor. Soc.*, **95** (9), S3–S6, doi:10.1175/1520-0477-95.9.S1.1.

Trenberth, K., G. W. Branstator, D. Karoly, A. Kumar, N. Lau, and C. Ropelewski, 1998: Progress during TOGA in understanding and modeling global teleconnections associated with tropical sea surface temperature. *J. Geophys. Res.*, **103**, 14 291–14 324, doi:10.1029/97JC01444.

Wang, H., and S. Schubert, 2014: Causes of the extreme dry conditions over California during early 2013 [in "Explaining Extreme Events of 2013 from a Climate Perspective"]. *Bull. Amer. Meteor. Soc.*, **95** (9), S7–S10, doi:10.1175/1520-0477-95.9.S1.1.

Watson, P. A. G., A. Weisheimer, J. R. Knight, and T. N. Palmer, 2016: The role of the tropical West Pacific in the extreme Northern Hemisphere winter of 2013/14. *J. Geophys. Res.*, **121**, 1698–1714, doi:10.1002/2015JD024048.

Williams, A. P., and Coauthors, 2015: Correlations between components of the water balance and burned area reveal new insights for predicting forest-fire area in the southwest United States. *Int. J. Wildland Fire*, **24**, 14–26, doi:10.1071/WF14023.

Yu, L., X. Jin, and R. Weller, 2008: Multidecade global flux datasets from the Objectively Analyzed Air–Sea Fluxes (OAFlux) Project: Latent and sensible heat fluxes, ocean evaporation, and related surface meteorological variables. Tech. Rep., Woods Hole Oceanographic Institute OAFlux Project OA-2008-01, 64 pp. [Available online at http://oaflux.whoi.edu/publications.html.]